The Journal of Immunology

An Alternative Splicing of *Tupaia* STING Modulated Anti-RNA Virus Responses by Targeting MDA5-LGP2 and IRF3

Ling Xu, Dandan Yu, Li Peng, Yong Wu, Yu Fan, Tianle Gu, Yu-Lin Yao, Jin Zhong, Xinwen Chen and Yong-Gang Yao

J Immunol 2020; 204:3191-3204; Prepublished online 6 May 2020;
doi: 10.4049/jimmunol.1901320
http://www.jimmunol.org/content/204/12/3191

The Journal of Immunology is published twice each month by
The American Association of Immunologists, Inc.,
1451 Rockville Pike, Suite 650, Rockville, MD 20852

Print ISSN: 0022-1767 Online ISSN: 1550-6606.

An Alternative Splicing of *Tupaia* STING Modulated Anti-RNA Virus Responses by Targeting MDA5-LGP2 and IRF3

Ling Xu,*,†,‡ Dandan Yu,*,†,‡ Li Peng,* Yong Wu,* Yu Fan,* Tianle Gu,*,§ Yu-Lin Yao,*,§ Jin Zhong,¶ Xinwen Chen,‖ and Yong-Gang Yao*,†,‡,§,#

The stimulator of IFN genes (STING; also known as MITA, TMEM173, MPYS, or ERIS) is generally regarded as a key adaptor protein for sensing pathogenic DNA genomes. However, its role in RNA viral signaling as part of the innate immunity system remains controversial. In this study, we identified two isoforms of STING (a full-length *Tupaia* STING [tSTING-FL] and a *Tupaia* STING short isoform [tSTING-mini]) in the Chinese tree shrew (*Tupaia belangeri chinensis*), a close relative of primates. tSTING-FL played a key role in the HSV-1–triggered type I IFN signaling pathway, whereas tSTING-mini was critical for RNA virus-induced antiviral signaling transduction. tSTING-mini, but not tSTING-FL, interacted with tMDA5–tLGP2 and tIRF3 in resting cells. Upon RNA virus infection, tSTING-mini caused a rapid enhancement of the tMDA5–tLGP2-mediated antiviral response and acted earlier than tSTING-FL. Furthermore, tSTING-mini was translocated from the cytoplasm to the nucleus during RNA virus infection and promoted tIRF3 phosphorylation through tSTING-mini–tIRF3 interaction, leading to a restriction of viral replication. After the initiation of antiviral effect, tSTING-mini underwent rapid degradation by tDTX3L–tPAPR9 via k48-linked ubiquitination through a proteasome-dependent pathway. Our results have shown alternative isoforms of STING counteract RNA virus infection in different ways. *The Journal of Immunology*, **2020, 204: 3191–3204.**

The innate immune system is crucial for defending against infections and employs pattern recognition receptors to recognize pathogen-associated molecular patterns. Subsequently powerful cellular antiviral signaling events and triggered signal cascades lead to the production of type I IFN (1, 2). Mobilization of these immune factors leads to rapid and temporally regulated changes in the expression of the hundreds of genes involved in host defenses, cell migration, tissue repair and regulation of adaptive immunity (3). Stimulator of IFN genes (STING) (4) (also known as mediator of IRF3 activation [MITA (5)], plasma membrane tetraspanner [MPYS (6)], endoplasmic reticulum (ER) IFN stimulator [ERIS (7)], or transmembrane protein 173 (TMEM173) was independently characterized by different groups and has been generally regarded as a key adaptor protein for DNA virus-sensing pathways. STING acts downstream of the retinoic acid–induced gene-I (RIG-I) and mitochondrial antiviral-signaling protein (MAVS) and plays a role in innate immune responses to cytosolic RNA by initiating the IFN response (4, 5, 8, 9). Subsequent studies have linked STING to cytosolic nucleic acid ligands, including dsDNA and unique bacterial nucleic acids called cyclic dinucleotides (4, 10–13). STING can activate TANK-binding kinase 1 (TBK1), and the activated TBK1 phosphorylates IFN regulatory factor 3 (IRF3), which is a key transcription factor for the induction of IFN-β expression (4, 5, 14, 15). Knockdown of STING using RNA interference at the N terminus of STING reduced RNA virus controlling activity (4, 5). However, using STING-deficient mice failed to confirm the proposed connection between STING and RNA virus infection (16–18). As compared with its documented role in sensing pathogenic DNA genomes, the basis for the involvements of STING in controlling RNA viral signaling remains controversial (8, 10, 19, 20), although STING antagonists were discovered in many RNA viruses (10, 21–26).

Because of its close relationship to primates (27, 28), the Chinese tree shrew (*Tupaia belangeri chinensis*) has proven to be a good

*Key Laboratory of Animal Models and Human Disease Mechanisms of the Chinese Academy of Sciences and Yunnan Province, Kunming Institute of Zoology, Kunming, Yunnan 650223, China; †Center for Excellence in Animal Evolution and Genetics, Chinese Academy of Sciences, Kunming, Yunnan 650223, China; ‡Kunming Primate Research Center of the Chinese Academy of Sciences, Kunming Institute of Zoology, Chinese Academy of Sciences, Kunming 650223, Yunnan, China; §Kunming College of Life Science, University of Chinese Academy of Sciences, Kunming, Yunnan 650204, China; ¶Key Laboratory of Molecular Virology and Immunology, Institute Pasteur of Shanghai, Chinese Academy of Sciences, Shanghai 200031, China; ‖State Key Laboratory of Virology, Wuhan Institute of Virology, Chinese Academy of Sciences, Wuhan 430071, China; and #Kunming Institute of Zoology–Chinese University of Hong Kong Joint Laboratory of Bioresources and Molecular Research in Common Diseases, Chinese Academy of Sciences, Kunming, Yunnan 650223, China

ORCIDs: 0000-0003-4769-935X (Y.W.); 0000-0002-5978-5004 (Y.F.); 0000-0002-3554-1275 (J.Z.); 0000-0002-4052-8155 (X.C.); 0000-0002-2955-0693 (Y.-G.Y.).

Received for publication October 31, 2019. Accepted for publication April 15, 2020.

This work was supported by the National Natural Science Foundation of China (U1402224, U1902215, and 81571998), the West Light Foundation of the Chinese Academy of Sciences (Light of West China Program xbzg-zdsys-201909) and the Yunnan Department of Science and Technology, Applied Basic Research Foundation of Yunnan Province (Yunnan Province Applied and Basic Research Foundation) (2016FB028 and 2018FB046).

Address correspondence and reprint requests to Dr. Yong-Gang Yao, Kunming Institute of Zoology, Chinese Academy of Sciences, Kunming 650223, Yunnan, China. E-mail address: yaoyg@mail.kiz.ac.cn

The online version of this article contains supplemental material.

Abbreviations used in this article: CAS, Chinese Academy of Sciences; c-di-GMP, cyclic dimeric GMP; ER, endoplasmic reticulum; HA, hemagglutinin; ISD, IFN stimulatory DNA; KIZ, Kunming Institute of Zoology; KO, knockout; 3-MA, 3-methyladenine; MAVS, mitochondrial antiviral-signaling protein; MOI, multiplicity of infection; NDV, Newcastle disease virus; RIG-I, retinoic acid–induced gene-I; RT-qPCR, real-time quantitative PCR; SeV, Sendai virus; siRNA, small-interfering RNA; sgRNA, single guide RNA; STING, stimulator of IFN genes; TBK1, TANK-binding kinase 1; tLGP2, *Tupaia* laboratory of genetics and physiology 2; TM, transmembrane motif; tMDA5, *Tupaia* melanoma differentiation-associated protein 5; TMEM173, transmembrane protein 173; TSPRC, tree shrew primary renal cell; tSTING, *Tupaia* STING; tSTING-FL, full-length *Tupaia* STING; tSTING-mini, short isoform *Tupaia* STING; VSV, vesicular stomatitis virus.

model for studying infectious diseases (29, 30) and for understanding the adaptation and functional diversity of antiviral activity in vertebrates (27, 31–33). For example, many studies have reported that the tree shrew was susceptible to hepatitis B virus and hepatitis C virus (34–39), HSV-1 (30), Zika virus (40), and influenza H1N1 virus (41). In this study, we characterized the STING ortholog from the Chinese tree shrew as having two isoforms, designated as full-length *Tupaia* STING (tSTING-FL) and short isoform *Tupaia* STING (tSTING-mini). tSTING-mini is part of the antiviral signaling after RNA virus infection acting with *Tupaia* melanoma differentiation-associated protein 5 (tMDA5)–*Tupaia* laboratory of genetics and physiology 2 (tLGP2). tSTING-mini facilitates IRF3 phosphorylation upon RNA virus infection, whereas tSTING-FL has a major role in anti-DNA virus response. Our study has revealed the diverse roles of the STING-mediated antiviral signaling via its isoforms in the Chinese tree shrew and has shown *Tupaia* STING (tSTING) restricts RNA virus replication by the phenomenon of alternative splicing.

Materials and Methods

Ethics statement

Animal experimental procedures and protocols were approved by the Institutional Animal Care and Use Committee of Kunming Institute of Zoology (KIZ), Chinese Academy of Sciences (CAS) (Approval No: SYDW20110315001) in accordance with the regulations in the Guide for the Care and Use of Laboratory Animals issued by the Ministry of Science and Technology of China.

Reagents and Abs

Poly(dA:dT) (catalog no. tlrl-patn), cyclic dimeric GMP (c-di-GMP; catalog no. tlrl-cdg), and IFN stimulatory DNA (ISD; catalog no. tlrl-isdn) were purchased from InvivoGen (San Diego, CA). The following Abs were used in this study: mouse monoclonal anti-Flag (M20008; Abmart), mouse anti–c-Myc (9E11) (MA1-16637; Life Technologies), mouse monoclonal anti-hemagglutinin (HA) (3724; Cell Signal Technology), mouse monoclonal anti-His (MA121315; Thermo Fisher Scientific), rabbit monoclonal anti-IRF3 (4302; Cell Signal Technology), rabbit monoclonal anti–phospho-IRF3 (Ser396) (4947; Cell Signal Technology), mouse monoclonal anti-GAPDH (E12-052-4; EnoGene), rabbit monoclonal anti-Histone H3 (4499; Cell Signal Technology), rabbit polycloncal tPARP9 (17535; Proteintech), rabbit polyclonal tDTX3L (11963; Proteintech), mouse monoclonal anti–β-actin (E1C602-2; EnoGene), mouse monoclonal anti–β-Tubulin (ZM-0439; Origene), and rabbit polyclonal anti-TMEM173 (LS-B7237; LifeSpan BioSciences; the epitope of this Ab was located in the region from the 50th to the 100th residue of human STING and was used to detect both tSTING-FL and tSTING-mini). Detection for phospho-p65 (Ser536) and p65 were performed by using the NF-κB pathway sample kit (9936; Cell Signal Technology). Peroxidase-conjugated anti-mouse Ab (474-1806; KPL) and anti-rabbit Ab (074-1506; KPL), FITC-conjugated anti-rabbit IgG (A21207; Life Technologies), and anti-mouse IgG (A21202; Invitrogen) were used as secondary Abs. Restriction enzymes *Eco*R I, *Xho* I, *Bsp*E I, *Sac* I, and *Hin*d III were purchased from Thermo Fisher Scientific.

Cell lines, viruses, and experimental animals

Vero (from African green monkey kidney) and HEK293T cells were supplied by the Kunming Cell Bank, KIZ, CAS. Cells were grown in DMEM (11965-092; Life Technologies-BRL) supplemented with 10% FBS (10099-141; Life Technologies-BRL) and 1× penicillin/streptomycin (10378016; Life Technologies-BRL) at 37°C in 5% CO_2. Chinese tree shrew primary renal cells (TSPRCs) were isolated and cultured according to the method of enzyme-assisted dissection as described previously (42, 43). RNA viruses (including Sendai virus [SeV], GFP-tagged vesicular stomatitis virus [VSV], Newcastle disease virus [NDV]), and DNA virus (HSV-1) were taken from our previous study (31). The Chinese tree shrews ($n = 30$) were purchased from the experimental animal core facility of KIZ, CAS. After euthanasia, seven different tissues (heart, liver, spleen, lung, kidney, intestine and brain) were dissected and frozen in liquid nitrogen, or the animals were used for isolating primary cells.

RNA interference and transfection

The small-interfering RNAs (siRNAs) targeting tSTING-FL or tSTING-mini and the negative control siRNA (Scramble) were obtained from RiboBio (Guangzhou, China). We designed three siRNAs for each of tSTING-FL, tSTING-mini, sitPARP9, and sitDTX3L, and evaluated the knockdown efficiency of each siRNA, respectively. The efficient siRNA for *tSTING-FL* (sitSTING-FL: 5′-GCGCTAAGCATCCTCCTAA-3′) was located in exon 2, whereas the efficient siRNA for *tSTING-mini* (sitSTING-mini: 5′-CCTCCCAAACTCTTCTGC-3′) was located in a region covering exons 2 and 5. The efficient siRNAs for sitPARP9 and sitDTX3L were 5′-TGGCAGCTCTGTTGACTAA-3′ and 5′-AGTACAACACTCACAGTAA-3′, respectively. TSPRCs were transfected according to the procedure in our previous study (31). In brief, cells (1×10^5 per well) were seeded in 12-well plates to grow to 50% confluence. Before transfection, culture medium was removed and washed once with Opti-MEM (31985-070; Life Technologies-BRL). The indicated siRNAs or Scramble was dissolved in Opti-MEM and was then mixed with 50 μl Lipofectamine 3000 (L3000008; Invitrogen) to achieve a final volume of 100 μl. After incubation at room temperature for 20 min, the siRNA–Lipofectamine mixture was added to each well, together with 400 μl Opti-MEM. After an incubation period of 6 h in the CO_2 incubator (Thermo Fisher Scientific), the medium was removed, and 1 ml growth medium was added to each well for 48 h. The inhibition efficiency of each siRNA was determined by real-time quantitative PCR (RT-qPCR) or Western blotting.

Total RNA extraction and quantification

Total RNA was extracted from tissues or primary renal cells using the RNAsimple Total RNA Kit (DP419; TIANGEN, Beijing, China) according to the manufacturer's instruction. We followed the procedure in our previous studies (32, 42, 43) to evaluate the quality and integrity of total RNA and perform the RT-qPCR. In brief, we used 1 μg total RNA to synthesize cDNA by using oligo-dT18 primer and M-MLV reverse transcriptase (M1701; Promega). RT-qPCR was performed using iTaq Universal SYBR Green Supermix (172-5125; Bio-Rad) supplemented with gene specific primers (Supplemental Table I) on a CFX Connect Real-Time PCR Detection system (Bio-Rad Laboratories, Hercules, CA) with the following thermal cycling condition: 1 cycle at 95°C for 1 min, 40 cycles of 95°C for 15 s, and 55°C for 15 s. The reaction volume (20 μl) contained 0.4 μM of each upstream and downstream primer (Supplemental Table I), 1 μl of cDNA, and 10 μl of iTaq Universal SYBR Green Supermix. The tree shrew *β-actin* gene was used as the reference for normalization of the target gene.

Establishment of CRISPR/Cas9-mediated tSTING knockout cell lines

We used the CRISPR/Cas9 system (44) to knock out the *tSTING* gene in TSR6 cells (45). The single guide RNAs (sgRNAs; tSTING-sgRNA-F1 5′-CACCGCCGTGGAATGGACGGATGC-3′/tSTING-sgRNA-R1 5′-AAACGCATCCGTCCATTCCACGGC-3′) targeted the exon 1 of *tSTING*. Briefly, the sgRNA pair was annealed and cloned into the pX330-T7 vector (a kind gift from Dr. P. Zheng, KIZ) expressing mCherry. The TSR6 cells were transfected with the pX330-T7 vector carrying the sgRNAs. Transfected cells expressing mCherry were sorted by flow cytometry and cultured for 48 h. Single cells were manually picked with a mouth pipette for expansion for 3 wk. The AxyPrep Multisource Genomic DNA Miniprep Kit (26817KC1; Axygen) was used to extract genomic DNA of single TSR6 cells with potential knockout of tSTING. The gene region spanning the sgRNA targeting sites was amplified by using primer pair tSTING-sgRNA-Fc 5′-GAGGGACTGTGCATGGGCAG-3′/tSTING-sgRNA-Rc 5′-GAGGCCAGGTGGAGCACCAG-3′. The PCR products were sequenced by using the primer tSTING-sgRNA-Fc to screen for mutation(s). We were able to pick up a cell clone (tSTING-knockout [KO] no. 3) with a frameshift mutation (c.37 insA) that disrupts the translation of tSTING protein. We used the anti-TMEM173 polyclonal Ab to probe the endogenous tSTING.

Plasmid construction

The coding regions of tSTING-FL and tSTING-mini were amplified and cloned into pEGFP-N2 with *Eco*R I and *Sac* I, pCMV-HA vector with *Eco*R I and *Xho* I, and cMyc-tagged pCS-myc-N vector with *Bsp*E I and *Xho* I, respectively (Supplemental Table I). The tree shrew *IFNB1* promoter luciferase reporter (IFN-β-Luc: pGL3-tIFN-β-promoter), ISRE-Luc (219092, ISRE *cis*-reporter; Stratagene) and NF-κB-Luc (631912, pNFκB-TA-Luc; Clontech), and pRL-SV40-*Renilla* (as an internal control; Promega) were described in our previous studies (31, 43). Expression vectors for tMDA5, tLGP2, and tMAVS were from our previous study (31). Expression vectors for tTBK1, tIRF3, tPARP9, and tDTX3L were generated using specific primer pairs and were cloned into indicated vectors (Supplemental Table I). All plasmids were verified by direct sequencing.

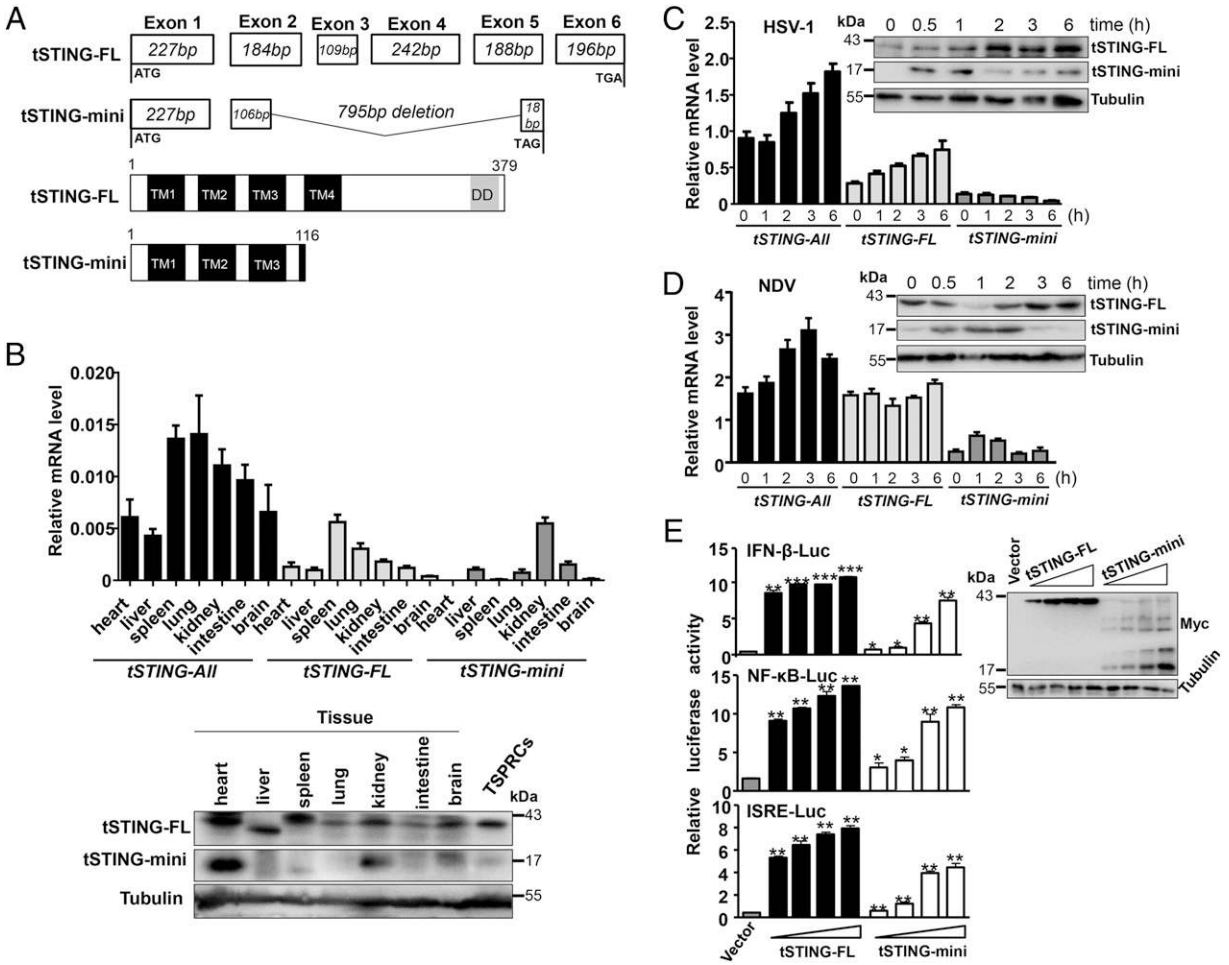

FIGURE 1. Genomic structure and expression pattern of the *STING* gene in the Chinese tree shrew. (**A**) Schematic sequence (upper) and domain structure (below) of tree shrew tSTING-FL and short STING (tSTING-mini). (**B**) The mRNA and protein levels of *tSTING* in seven tissues from the Chinese tree shrew. (Upper) The RT-qPCR results (n = 10 animals, mean ± SEM) for *tSTING* transcripts. RT-qPCR was determined by using sequence-specific primers and was normalized by *β-actin*. (Below) Protein levels of the two tSTING isoforms in different tissues (each 50 μg; tree shrew tissues were from two individuals) and TSPRCs (150 μg) were detected by anti-TMEM173 Ab. The tubulin was used as the loading control. The Western blot was repeated four times, with similar results. *tSTING-All* refers to the result of the primer pair that captures both *tSTING-FL* and *tSTING-mini*. (**C** and **D**) Time-dependent alterations of *tSTING* mRNA and protein levels in TSPRCs during HSV-1 (C) and NDV (D) infection. Cells (1×10^5) were grown in the 12-well plates overnight, followed by infection with HSV-1 (MOI = 10) or NDV (MOI = 1) for indicated times before the harvest. The procedure for detecting *tSTING* transcripts (n = 3 replicates per group, mean ± SEM) and protein levels was similar to (B). (**E**) Activation of the IFN-β-Luc, NF-κB-Luc, and ISRE-Luc reporters by tSTING isoforms in TSPRCs. (left) Cells (1×10^4) were transfected with the respective reporter vector and increased amount (3.2, 16, 80, and 400 ng) of tSTING-FL or tSTING-mini expression vector (with empty vector to reach a total amount of 400 ng) for 48 h before the luciferase assay (n = 3 replicates per group, mean ± SEM). (right) Immunoblot analysis showing successful dose-dependent overexpression of tSTING-FL and tSTING-mini in TSPRCs. Ab for Myc was used for detecting tSTING-FL and tSTING-mini. Tubulin was used as a loading control. All data in (C)–(E) are representative of three independent experiments with similar results. $*p < 0.05$, $**p < 0.01$, $***p < 0.001$, relative to empty vector group, two-tailed Student t test.

Lentiviral infection system for STING

We generated a lentiviral expression system for tSTING-FL or tSTING-mini by using the HEK293T cells. Briefly, cells were seeded into six-well plates at a density of 4×10^5 cells per well and cotransfected with 0.4 μg of pMD2.G (12259; Addgene), 0.8 μg of psPAX2 (12260; Addgene), and 1.3 μg of pLVX-IRES-Neo (632181; Clontech) with tSTING-FL or tSTING-mini, respectively. The viral supernatants were harvested and filtered with 0.45-μm filters at 48 h posttransfection.

For lentiviral infection, tSTING-deficient TSR6 cells (tSTING-KO) were seeded in six-well plates at a density of 4×10^5 cells per well. After 12 h, the culture medium was replaced by infection mixture (500 μl culture medium with 1 μg polybrene [H8761; Solarbio] and 500 μl viral supernatants). G418 (11811023, 0.5 μg/ml; Thermo Fisher Scientific) was added to the culture medium at 48 h postinfection, and the G418-resistant cells were pooled and expanded.

Luciferase reporter assay

TSPRCs were plated in 24-well plates at a density of 1×10^4 cells and cultured overnight. Cells were transfected with 0.1 μg of the luciferase reporter vector, 0.01 μg pRL-SV40-Renilla, together with the indicated mounts of an empty vector (Mock) or indicated expression vector using X-tremeGENE HP DNA Transfection Reagent (06366236001; Roche). After transfection for 36 h, cells were left untreated or infected with SeV (20 hemagglutination unit/ml), NDV (multiplicity of infection [MOI] = 1) for 12 h, or HSV-1 (MOI = 1) for the indicated times. Cells were harvested for luciferase activity by using the Dual-Luciferase Reporter Assay System (E1960; Promega) on an Infinite M1000 Pro multimode microplate reader (30064852; Tecan).

Immunofluorescence analysis and flow cytometry

TSPRCs were seeded on glass coverslips and grown overnight to 40% confluence in DMEM supplemented with 10% FBS at 37°C in 5% CO_2. After transfection with the indicated vectors for 36 h, cells were left untreated or infected with DNA virus (HSV-1) for 2 h or RNA virus (NDV) for the indicated times. For immunofluorescence analysis, cells were fixed with 4% paraformaldehyde for 10 min for direct imaging by an Olympus FluoView 1000 confocal microscope (Olympus, America) or were incubated with mouse anti-Flag (1:500), anti-HA (1:500), anti-IRF3 (1:500), anti-tPARP9 (1: 500), or anti-tDTX3L (1: 500) overnight at 4°C. After

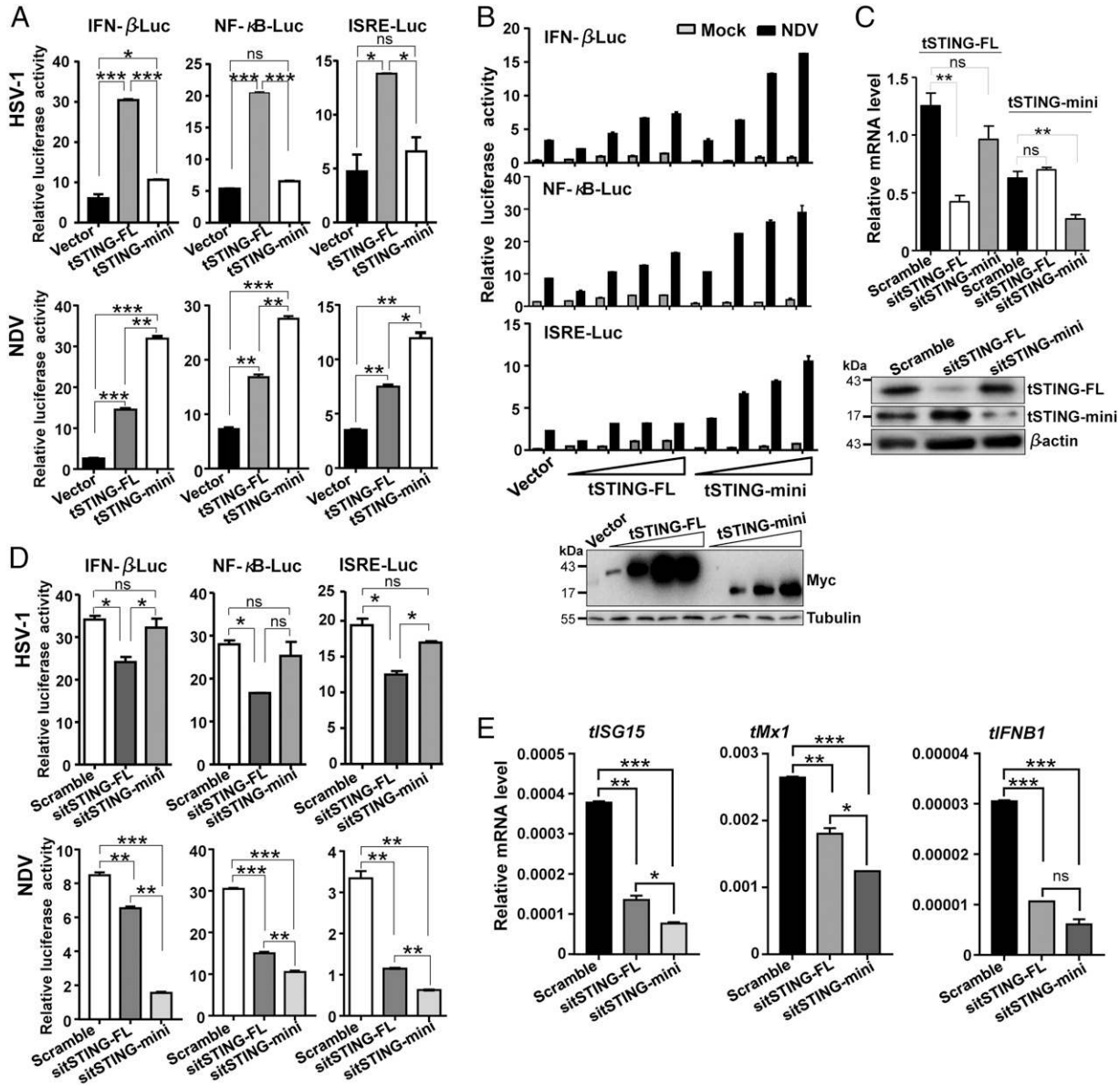

FIGURE 2. The two STING isoforms play different roles in TSPRCs in response to NDV and HSV-1 infections. (**A**) Effect of tSTING-FL or tSTING-mini overexpression on the IFN-β-Luc, ISRE-Luc, and NF-κB-Luc reporters in response to NDV or HSV-1 infection. TSPRCs (1×10^4) were cotransfected with the expression vector for tSTING-FL (400 ng) or tSTING-mini (400 ng), indicated luciferase reporter vector (100 ng), and TK (10 ng, as an inner control) for 36 h, followed by NDV infection (MOI = 1) or HSV-1 (MOI = 10) for 12 h before the harvest. (**B**) Dose-dependent activation effect of tSTING-mini but not tSTING-FL overexpression on the IFN-β-Luc, ISRE-Luc, and NF-κB-Luc reporters in TSPRCs infected with NDV. The procedure was similar to (A), except for using increased amount (3.2, 16, 80, and 400 ng) of tSTING-FL or tSTING-mini expression vector (with empty vector to reach a total amount of 400 ng). The inserted immunoblot showed successful overexpression of tSTING-FL and tSTING-mini in TSPRCs. (**C**) Knockdown efficiency of tSTING–siRNAs. TSPRCs (1×10^5) were transfected with siRNA negative control (Scramble, 50 nM), sitSTING-mini (50 nM), or sitSTING-FL (50 nM) for 24 h and harvested for measuring *tSTING* mRNA (upper) and protein (below) levels. The procedure was similar to Fig. 1B. (**D**) Effect of tSTING-FL or tSTING-mini knockdown on the IFN-β-Luc, ISRE-Luc, and NF-κB-Luc reporter activities induced by NDV or HSV-1 infection. Procedure was similar to (A), with the replacement of expression vector with siRNA negative control (Scramble, 50 nM), sitSTING-FL (50 nM) or sitSTING-FL (50 nM) for 24 h. (**E**) Knockdown of tSTING-mini, but not tSTING-FL, significantly decreases NDV-induced *tIFNB1*, *tISG15*, and *tMx1* mRNA levels in TSPRCs. Cells (1×10^5) were transfected with the siRNA negative control (Scramble, 50 nM), sitSTING-FL (50 nM), or sitSTING-mini (50 nM) for 24 h, followed by NDV infection (MOI = 1) for 12 h before the harvest. The values in (A)–(E) are mean ± SEM ($n = 3$ replicates per group). All data in (A)–(E) are representative of three independent experiments with similar results. $^*p < 0.05$, $^{**}p < 0.01$, $^{***}p < 0.001$, two-tailed Student *t* test.

three washes with PBS (5 min each), immunoreactivity was detected by using the FITC-conjugated secondary Ab (1:500; KPL, 172-1506; incubation for 1 h at room temperature). Nuclei were counterstained with 1 μg/ml DAPI (10236276001; Roche Diagnostics), and the slides were visualized under an Olympus FluoView 1000 confocal microscope.

For measuring replication of VSV-GFP, flow cytometry analysis was performed as described in our previous study (31). Briefly, cells were infected with VSV after indicated times and were fixed in 4% paraformaldehyde in PBS (pH 7.4). Percentage of 10,000 cells expressing GFP (GFP^+ cells) was counted by flow cytometry. The flow cytometry data were analyzed by FlowJo v10.0.7 software.

Western blotting and immunoprecipitation

We followed the procedures for Western blotting and immunoprecipitation in our previous study (31). In brief, TSPRCs were seeded in 10-cm plates at 70% confluence and were transfected with the indicated vectors using X-tremeGENE HP DNA Transfection Reagent (06366546001; Roche). Cells were lysed on ice in RIPA lysis buffer (P0013; Beyotime Institute of

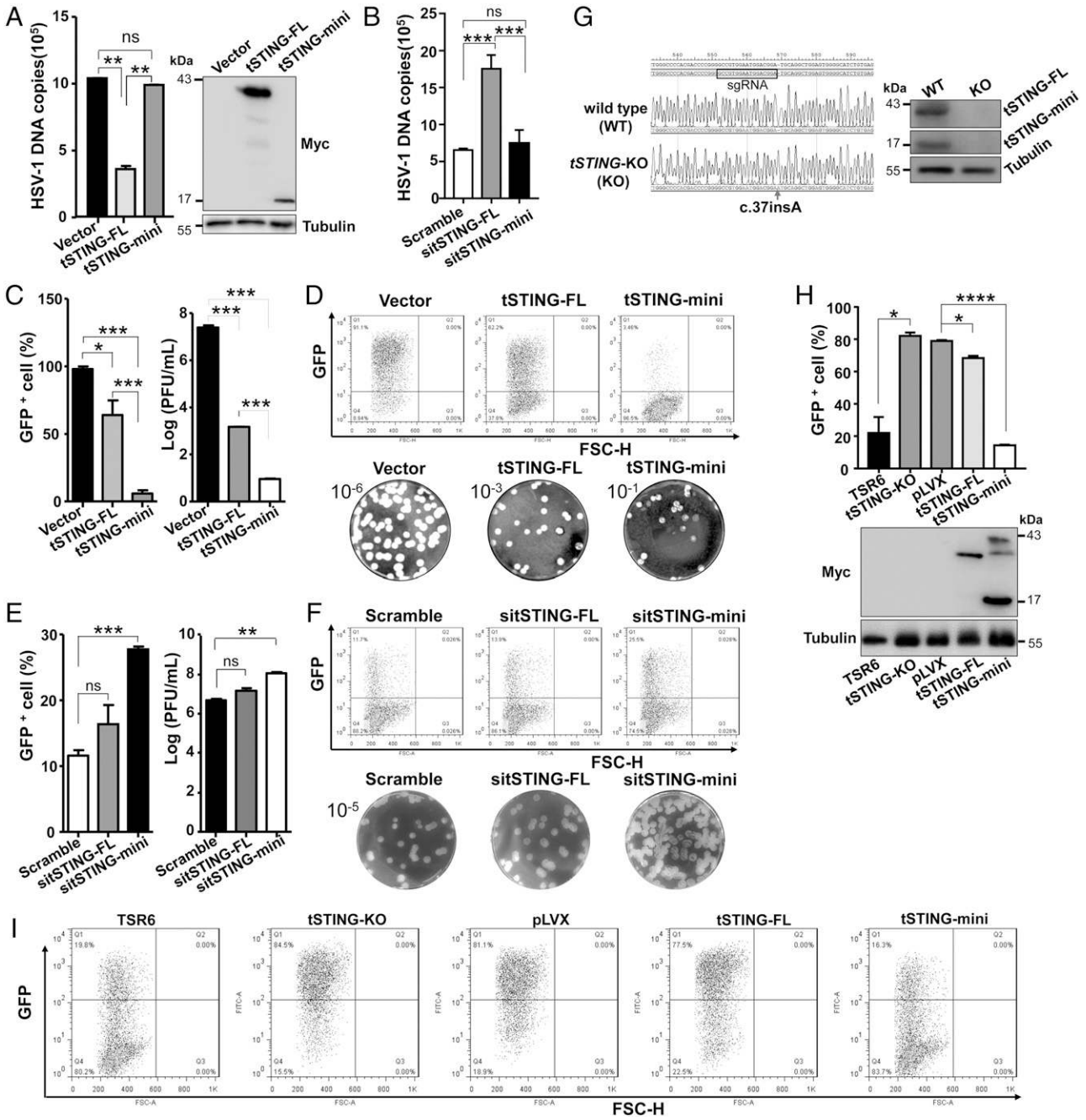

FIGURE 3. The effect of overexpression or knockdown of tSTING isoforms on the replication of VSV and HSV-1. (**A**) Effect of tSTING-FL or tSTING-mini overexpression on HSV-1 DNA copies in the supernatants of TSPRCs infected with HSV-1. TSPRCs (1×10^5) were transfected with the indicated expression vector or empty vector (each 1 μg) for 12 h before HSV-1 infection (MOI = 10) for 1 h. Cells were washed with PBS seven times and switched to growth medium for 36 h. The culture medium was collected to quantify the HSV-I DNA copies by using RT-qPCR. The immunoblot on the right showed successful overexpression of tSTING-FL and tSTING-mini in TSPRCs. (**B**) Knockdown of tSTING-FL promotes HSV-1 DNA copies in TSPRCs infected with HSV-1. TSPRCs (1×10^5) were transfected with the siRNA negative control (Scramble, 50 nM), sitSTING-FL (50 nM), or sitSTING-mini (50 nM) for 24 h. The subsequent procedure and conditions were the same as (A). (**C**) Overexpression of tSTING inhibits VSV replication in TSPRCs. Cells (1×10^5) were transfected with the indicated expression vector or empty vector (each 1 μg) for 12 h and infected with VSV (MOI = 0.01) for 12 h. (left) The percentage of VSV-GFP–positive cells (GFP^+ cells) in cells transfected with empty vector (Vector) or tSTING isoform. (Right) The VSV titers in the supernatants of transfected cells were analyzed by standard plaque assay. (**D**) Flow cytometry analysis of cells and VSV plaque assay in (C). (Upper) Percentage of 10,000 cells expressing GFP (GFP^+ cells) was counted by flow cytometry. (Below) Vero cells were infected with different dilutions of VSV in the culture supernatant of infected TSPRCs (10^{-6} for cells transfected with empty vector, 10^{-3} for cells transfected with tSTING-FL, and 10^{-1} for cells transfected with tSTING-mini). (**E**) Knockdown of tSTING-mini increases VSV replication in TSPRCs. Cells (1×10^5) were transfected with the siRNA negative control (Scramble, 50 nM), sitSTING-FL (50 nM), and sitSTING-mini (50 nM) for 24 h, followed by VSV infection for 12 h before the harvest. The procedure was similar to (C). (**F**) Flow cytometry analysis of cells and VSV plaque assay in (E). The procedure was similar to (D). (**G**) Identification of the tSTING knockout cells. (left) Sequencing chromatographs showing the frameshift mutation (c.37insA) in *tSTING* in TSR6 knockout cells (tSTING-KO). (right) Immunoblot analysis showing no endogenous tSTING protein in tSTING-KO cells. (**H** and **I**) Stable expression of tSTING-FL or tSTING-mini in tSTING-KO cells rescued the ability to restrict VSV replication. The TSR6, tSTING-KO, and STING-KO cells with lentiviral transfection for empty vector (pLVX), tSTING-FL, or tSTING-mini (each 1×10^5 cells) were infected with VSV (MOI = 0.01) for 12 h, respectively. *(Figure legend continues)*

Biotechnology) and were centrifuged at 12,000 × *g*, 4°C for 5 min to harvest the cell lysates. Protein concentration was determined by using the BCA protein assay kit (P0012; Beyotime Institute of Biotechnology). BSA (P0007; Beyotime Institute of Biotechnology) was used as a protein standard. Cell lysates (20 μg total protein per sample) were separated by electrophoresis on 12% SDS-PAGE and were transferred to polyvinylidene fluoride (PVDF) membranes (IPVH00010; Roche Diagnostics) using the standard procedure. The membranes were blocked with 5% nonfat dry milk in TBST (TBS [no. 9997; Cell Signaling Technology] with Tween 20 [P1379, 0.1%; Sigma-Aldrich]) at room temperature for 2 h. Membranes were incubated with respective primary Abs against Myc (1:5000), STING (1: 500), Flag (1:5000), HA (1:5000), IRF3 (1:1000), phospho-IRF3 (Ser396) (1:1000), phospho-p65 (Ser536) (1:1000), p65 (1:1000), Histone H3 (1:2000), PARP9 (1:1000), DTX3L (1:1000), GAPDH (1:10,000), Tubulin (1:10,000), and β-actin (1:10,000) overnight at 4°C. Membranes were washed three times (5 min each) and were incubated with TBST-conjugated anti-mouse or anti-rabbit secondary Ab (1:10,000) for 1 h at room temperature. After another round of three washes with TBST, proteins on the membranes were detected by using ECL reagents (WBKLS0500; Millipore).

For immunoprecipitation, appropriate Abs were incubated with protein G-agarose beads (15920010; Life Technologies) to form a complex for 2 h at room temperature. Cells were lysed with the RIPA lysis buffer on ice for 1 h, followed by a centrifugation at 12,000 × *g* for 10 min at 4°C. Lysates were then immunoprecipitated with the complex at 4°C overnight, followed by four washes with the RIPA lysis buffer and were resuspended in loading sample buffer for SDS-PAGE.

VSV plaque assay

TSPRCs (2×10^5) were transfected with the indicated vectors, tSTING siRNA or scrambled siRNA for 12 h prior to VSV infection. Cells were washed with serum-free DMEM for three times at 1 h after VSV (MOI = 0.01) infection, then were grown in DMEM supplemented with 1% FBS. The culture supernatants were harvested at 16 h after virus infection and were serially diluted (10-fold) in serum-free DMEM to infect confluent Vero cells cultured on six-well plates. At 1 h postinfection, the supernatant was discarded, and 1% low–melting point agarose with growth medium (2 ml/well) was overlaid. At 3 d postinfection, the agarose was removed, and cells were fixed with 4% formaldehyde for 20 min and stained with 0.2% crystal violet (Beyotime Institute of Biotechnology). Plaques were counted, averaged, and multiplied by the dilution factor to determine viral titer as the number of PFU per sample unit volume.

Statistical tests

The ImageJ (National Institutes of Health, Bethesda, MD) was used to evaluate the densitometry of immunofluorescence. Comparisons between different groups were conducted by using two-tailed Student *t* test (PRISM software; GraphPad Software). Data are presented as mean ± SEM. A p value < 0.05 was considered as statistically significant.

Results

Identification of the STING ortholog in the Chinese tree shrew

The full length of *tSTING* transcript (*tSTING-FL*) is 1516 bp (https://www.ncbi.nlm.nih.gov/nuccore/KU998262), with a 223-bp 5′-untranslated region and a 153 bp 3′-untranslated region (excluding the poly-A tail). Similar to human STING, tSTING-FL has canonical functional domains, including four transmembrane motifs (TM) in the N-terminal (residue 1–137) and the C-terminal domain (residue 138–379), which are responsible for binding the cytosolic dinucleotides and recruiting the downstream factors (9, 10) (Fig. 1A, Supplemental Fig. 1A). In addition to this canonical transcript, we identified an alternative splicing variant of tSTING (designated as tSTING-mini, https://www.ncbi.nlm.nih.gov/nuccore/KU998263) in pooled total RNA from six tissues. The variant was the result of exon skipping and ended at a stop codon at nt 351 (Fig. 1A). tSTING-mini shared the same N-terminal portion with tSTING-FL up to the 111st residue and possessed a unique five-residue sequence at the C terminus. The tSTING-mini contained the first three TMs and the incomplete fourth TM of tSTING-FL (Fig. 1A, Supplemental Fig. 1A).

We used transcript-specific primer pairs to quantify the mRNA levels of *tSTING-FL* and *tSTING-mini* (Supplemental Fig. 1B, Supplemental Table I). We have shown that the spleen and lung had a relatively high mRNA level of whole *tSTING* (*tSTING-All*) and *tSTING-FL*, whereas the kidney tissue had the highest level of *tSTING-mini*. The mRNA level of *tSTING-mini* was barely detected in heart, spleen, and brain (Fig. 1B *upper*). The tSTING-FL protein was generally more abundant than the tSTING-mini protein in each tissue. Note that there was inconsistency regarding the mRNA and protein levels for tSTING in the heart and kidney (Fig. 1B below and Supplemental Fig. 1C). The tSTING-mini protein level was relatively higher in the heart and kidney, but not in immune compartment like spleen. We also found that the mRNA levels of *tSTING-All*, *tSTING-FL*, and *tSTING-mini* in the kidney tissue had some differences with those of cells derived from the kidney tissues, such as TSPRCs and TSR6 cells (Supplemental Fig. 1D).

To determine the different effects of tSTING after viral infection, we investigated the dynamics of tSTING-FL and tSTING-mini in TSPRCs in response to infection of DNA virus (HSV-1, Fig. 1C) or RNA viruses (NDV, Fig. 1D; SeV, Supplemental Fig. 1E), respectively. The mRNA and protein levels of tSTING-FL were increased in a time-dependent manner, whereas those of tSTING-mini were reduced during HSV-1 infection (Fig. 1C). Upon NDV infection, the mRNA level of tSTING-FL had no substantial change relative to the baseline level, but the protein level was decreased along with time and then increased at 2 h. The protein level of tSTING-mini was increased after NDV infection, with a peak level at 2 h, thereafter gradually returned to the basal level at the late time points (Fig. 1D). Upon SeV infection, the mRNA and protein levels of tSTING-FL had no significant change relative to the baseline level, whereas the mRNA and protein levels of tSTING-mini presented a similar pattern as that of NDV infection (Supplemental Fig. 1E).

We constructed tSTING expression vectors and explored their function in activating the IFN-β-Luc, ISRE-Luc, and NF-κB-Luc luciferase reporters. Overexpression of tSTING-FL or tSTING-mini in TSPRCs activated all three luciferase reporters in a dose-dependent manner (Fig. 1E). These results demonstrated that *tSTING-FL* and *tSTING-mini* had different structures and tissue expression patterns and could positively regulate the type I IFN induction.

tSTING-mini activated RNA virus-triggered IFN signaling

We determined whether tSTING-FL and tSTING-mini played different roles in activating the IFN-β-Luc, NF-κB-Luc, and ISRE-Luc luciferase reporters in TSPRCs in response to HSV-1 or RNA viruses (NDV and SeV) infection. Compared with the empty vector group, overexpression of tSTING-FL significantly potentiated HSV-1-induced activation of the three luciferase reporters, whereas it had a relatively weak activation effect in response to NDV (Fig. 2A) and SeV (Supplemental Fig. 2A) infections. The

The subsequent procedure and conditions were the same as (C). Results of flow cytometry analysis of the indicated cells were shown in (H), and the original flow cytometry data are shown in (I). The values in (A)–(C), (E), and (H) are mean ± SEM ($n = 3$ replicates per group). All data in (A)–(I) are representative of three independent experiments with similar results. $^*p < 0.05$, $^{**}p < 0.01$, $^{***}p < 0.001$, two-tailed Student *t* test.

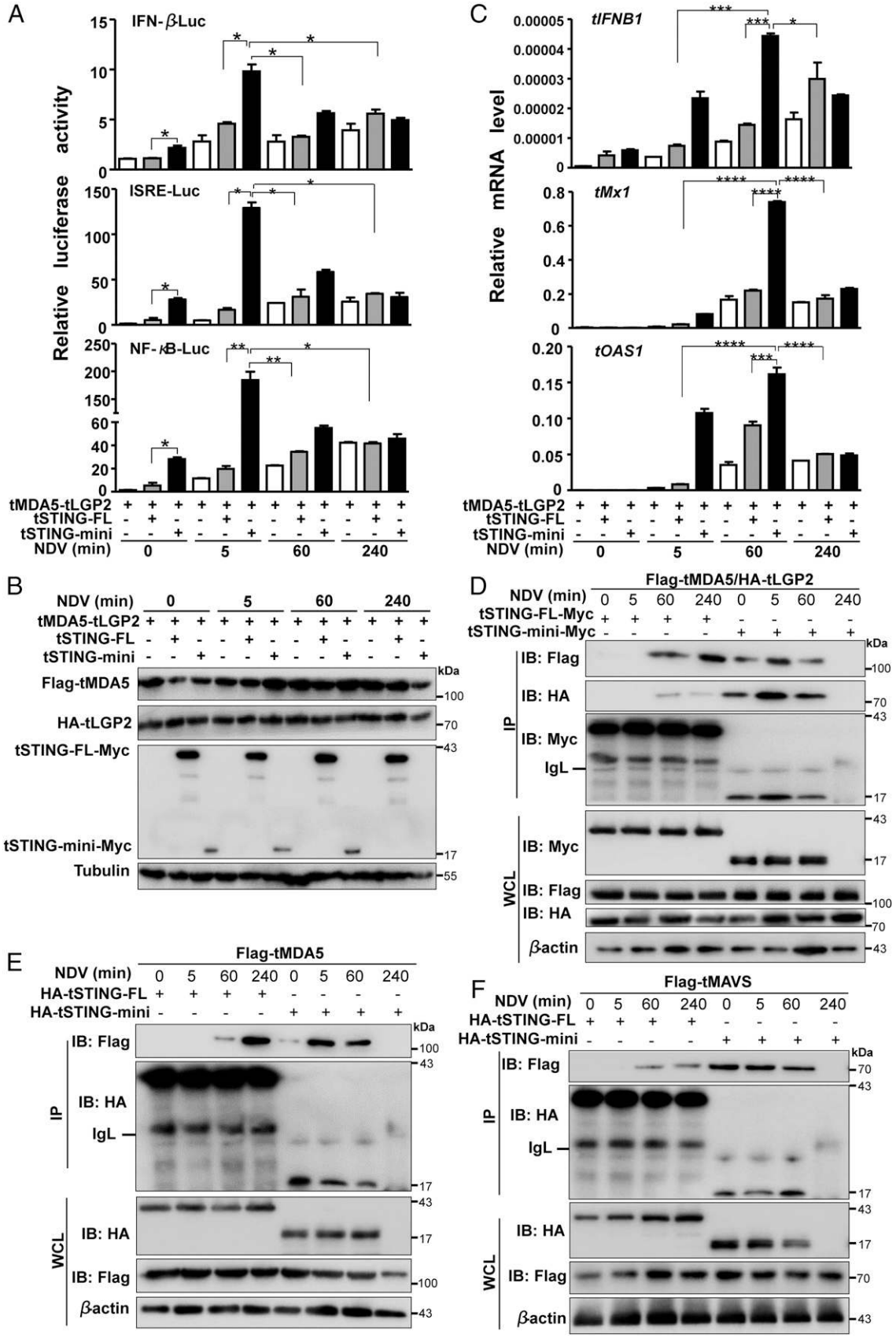

FIGURE 4. tSTING-mini interacts with tMDA5–tLGP2 and promotes IFN signaling. (**A**) Overexpression of tMDA5–tLGP2 activates the IFN-β-Luc, ISRE-Luc, and NF-κB reporters mediated by tSTING-mini. TSPRCs (1×10^4) were transfected with the indicated reporter (100 ng), TK (10 ng, as an inner control), expression vectors for tMDA5 (175 ng) and tLGP2 (25 ng), and expression vector for tSTING-mini or tSTING-FL (200 ng) for 48 h, followed by NDV infection (MOI = 1) for the indicated times before the luciferase analysis. (**B**) Immunoblot analysis showed successful overexpression of the indicated vectors in TSPRCs. (**C**) Overexpression of tMDA5–tLGP2 activates tSTING-mini–mediated upregulation of *tIFNB1*, *(Figure legend continues)*

enhancing effect of tSTING-FL overexpression on HSV-1–induced luciferase reporter activities was dose dependent (Supplemental Fig. 2B). Similar patterns were observed for stimulation with poly(dAT:dTA) (AT-rich dsDNA) (Supplemental Fig. 2C), ISD (non–AT-rich dsDNA) (Supplemental Fig. 2D), or c-di-GMP (Supplemental Fig. 2E) in TSPRCs overexpressing tSTING-FL. We observed a different activation effect in TSPRCs overexpressing tSTING-mini compared with tSTING-FL overexpression in response to HSV-1 or RNA virus (NDV and SeV) infection. NDV or SeV infection, but not HSV-1 infection, significantly activated the three luciferase reporters in TSPRCs overexpressing tSTING-mini relative to the empty vector group (Fig. 2A, Supplemental Fig. 2A). Moreover, NDV or SeV infection induced tSTING-mini–mediated IFN-β-Luc, NF-κB-Luc, and ISRE-Luc reporter activities in a dose-dependent manner, and this effect was more pronounced than that of tSTING-FL (Fig. 2B, Supplemental Fig. 2F, 2G). Overexpression of tSTING-mini in TSPRCs had a seemingly dose-dependent inhibitory effect on the three luciferase reporter activities upon HSV-1 infection (Supplemental Fig. 2B), poly(dAT:dTA) (Supplemental Fig. 2C), ISD (Supplemental Fig. 2D), or c-di-GMP (Supplemental Fig. 2E) stimulation. These observations indicated that tSTING-FL and tSTING-mini had different roles to counteract HSV-1 and RNA viruses (NDV and SeV) infections.

To determine the roles of endogenous tSTING-FL and tSTING-mini, we knocked down tSTING-FL and tSTING-mini by using siRNA in TSPRCs. We observed a reasonably good knockdown efficiency (up to 50%) for siRNAs specifically targeting the two tSTING transcripts, respectively (Fig. 2C). Knockdown of tSTING-FL significantly inhibited the HSV-1–induced activation of the IFN-β-Luc, ISRE-Luc, and NF-κB-Luc reporters relative to scramble cells (Fig. 2D). Furthermore, knockdown of tSTING-FL significantly inhibited HSV-1–induced transcription of endogenous *tISG15*, *tMx1*, and *tIFNB1* (Supplemental Fig. 2H). In contrast, knockdown of tSTING-mini by sitSTING-mini had no obvious effect on the HSV-1–induced activation of the three luciferase reporters but had a significant inhibition effect on the three luciferase reporter activities in TSPRCs infected with NDV or SeV (Fig. 2D, Supplemental Fig. 2I). This inhibitory effect could also be seen in the significant decrease of NDV- or SeV-induced mRNA levels of *tISG15*, *tMx1*, and *tIFNB1* in TSPRCs transfected with sitSTING-mini as compared with that of sitSTING-FL (Fig. 2E, Supplemental Fig. 2J). These results suggested that tSTING-mini might be preferentially involved in RNA virus infection.

We further examined the effects of tSTING-FL and tSTING-mini on viral replication. We observed a significant decrease of HSV-1 copy in TSPRCs overexpressing tSTING-FL but not tSTING-mini (Fig. 3A). Conversely, knockdown of tSTING-FL significantly increased HSV-1 copies, whereas tSTING-mini knockdown had no such an effect (Fig. 3B). As indicated by the diminished GFP expression, overexpression of tSTING-FL or tSTING-mini could inhibit GFP-tagged VSV (VSV-GFP) replication in TSPRCs, but the inhibitory effect was more striking for tSTING-mini (Fig. 3C, 3D). Further quantification of viral titers confirmed the stronger inhibitory effect of tSTING-mini over tSTING-FL (Fig. 3D). Knockdown of tSTING-FL or tSTING-mini increased VSV-GFP replication in the TSPRCs, with the best effect for sitSTING-mini (Fig. 3E, 3F).

We generated tSTING-deficient TSR6 cells (tSTING-KO) by using the CRISPR/Cas9 method (Fig. 3G). The replication of VSV-GFP was significantly enhanced in tSTING-KO cells in comparison with wild-type TSR6 cells (Fig. 3H). Introduction of tSTING-FL or tSTING-mini back into tSTING-KO cells showed that tSTING-FL could inhibit VSV-GFP replication, whereas tSTING-mini had a greater inhibition effect compared with tSTING-KO cells transfected with pLVX (negative control) or tSTING-FL (Fig. 3H, 3I). Taken together, these results suggested that tSTING-mini played an active role in antiviral response to RNA virus but not DNA virus infection. Conversely, tSTING-FL maintained its canonical function for anti-DNA virus infection and had an inferior effect on anti-RNA virus infection compared with tSTING-mini.

tSTING-mini interacted with tMDA5–tLGP2 and promoted the IFN signaling in response to RNA viruses

We recently found the Chinese tree shrew lacks RIG-I (27, 31). With the help of tLGP2, tMDA5 partially replaced the function of RIG-I to sense RNA virus (31). We examined whether tSTING-mini was involved in the tMDA5–tLGP2-mediated signaling in TSPRCs to enhance antiviral activity via the RNA virus-induced signaling. In transient transfection and reporter assays, overexpression of tSTING-mini significantly enhanced the activation of the IFN-β-Luc, ISRE-Luc, and NF-κB-Luc reporters induced by tMDA5–tLGP2, compared with tSTING-FL (Fig. 4A). tSTING-mini had a rapid induction effect and remarkably increased the luciferase activities at 5 and 60 min after NDV infection, followed by a return to the resting state at 4 h (Fig. 4A, 4B). Similarly, overexpression of tSTING-mini together with tMDA5 and tLGP2 significantly enhanced the NDV-induced upregulation of downstream genes *tIFNB1*, *tMx1*, and *tOAS1* (Fig. 4C).

Immunoprecipitation of tagged proteins showed that tSTING-mini bound to tMDA5–tLGP2 in uninfected cells, and this association was increased at 5 min after NDV infection (Fig. 4D). The interaction of tSTING-mini and tMDA5–tLGP2 was greatly reduced along with the degradation of tSTING-mini at 4 h in NDV-infected TSPRCs (Fig. 4D). In contrast, overexpressed tSTING-FL did not bind to tMDA5–tLGP2 in resting TSPRCs, but we observed a time-dependent increase of association between tSTING-FL and tMDA5–tLGP2 in TSPRCs after NDV infection (Fig. 4D). These data suggested that tSTING-mini regulated the RNA virus-induced signaling mediated by tMDA5–tLGP2 in a rapid manner. We observed an association of tSTING-mini or tSTING-FL with tMDA5, similar to the pattern for association with tMDA5–tLGP2 during NDV

tOAS1, and *tMx1* mRNA levels in TSPRCs by using RT-qPCR. Cells (1×10^5) were transfected with expression vectors for tMDA5 (400 ng) and tLGP2 (100 ng) and expression vector for tSTING-FL (500 ng) or tSTING-mini (500 ng) for 36 h, followed by NDV infection (MOI = 1) for the indicated times before the harvest. The values in (**A**) and (**C**) are mean ± SEM ($n = 3$ replicates per group). (**D**) tSTING interacts with tMDA5–tLGP2. TSPRCs (1×10^7) were cotransfected with expression vectors for tSTING-FL–Myc or tSTING–mini-Myc (5 μg) and Flag-tMDA5 (4 μg)/HA-tLGP2 (1 μg) for 48 h, followed by NDV infection (MOI = 1) for the indicated times before the harvest. Whole-cell lysates (WCL) were immunoprecipitated (IP) by using anti-cMyc Ab. Immunoblots (IB) for tSTING (tSTING-FL and tSTING-mini), tMDA5, tLGP2, and β-actin were performed by using anti-cMyc, anti-Flag, anti-HA, and anti–β-actin Abs, respectively. (**E**) tSTING interacts with tMDA5. (**F**) tSTING interacts with tMAVS. The procedures for IP and IB in (E) and (F) were similar to (D). IgL, Ig L chain. All data in (A)–(F) are representative of three independent experiments with similar results. $^*p < 0.05$, $^{**}p < 0.01$, $^{***}p < 0.001$, $^{****}p < 0.0001$, two-tailed Student *t* test.

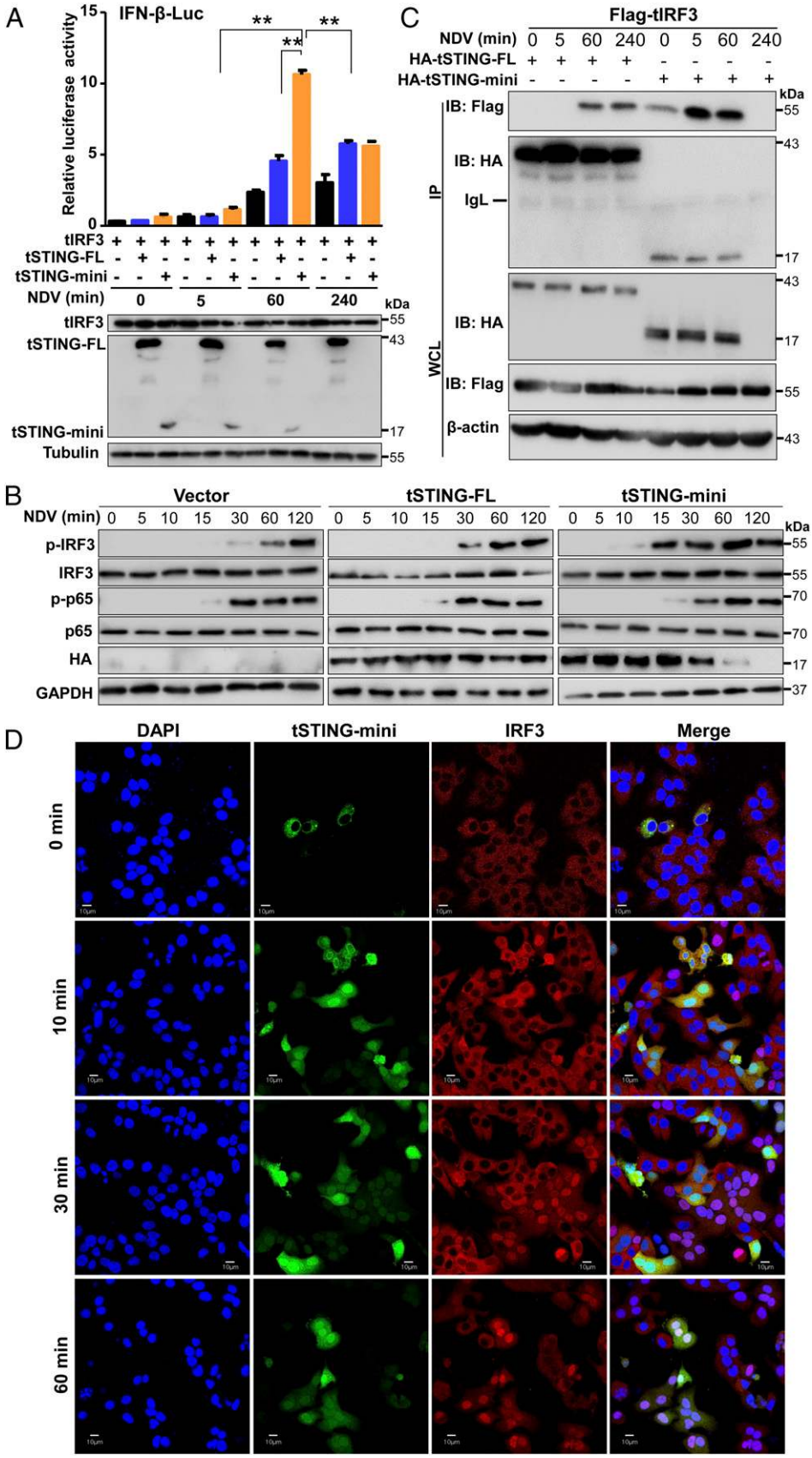

FIGURE 5. tSTING-mini promotes tIRF3 phosphorylation and interacts with tIRF3 in TSPRCs. (**A**) Overexpression of tSTING-mini activates tIRF3-mediated activation of the IFN-β-Luc reporter. (Upper) TSPRCs (1×10^5) were transfected with IFN-β-Luc reporter (100 ng), TK (10 ng), and expression vectors of tIRF3 (200 ng) and tSTING-FL (200 ng) or tSTING-mini (200 ng) for 48 h, followed by NDV infection (MOI = 1) at the indicated times ($n = 3$ replicates per group, mean ± SEM; $^{**}p < 0.01$, two-tailed Student t test). This assay was independently repeated three times and had consistent results. (Below) Immunoblot analysis showing successful overexpression of the indicated expression vectors in TSPRCs. (**B**) Overexpression of tSTING-mini promotes tIRF3 phosphorylation. TSPRCs (1×10^6) were transfected with empty vector (Vector, 2.5 μg), HA-tSTING-mini, or HA-tSTING-FL expression vector (2.5 μg) for 48 h, followed by infection with NDV (MOI = 1) at the indicated times. (**C**) tIRF3 interacts with tSTING-mini. TSPRCs (1×10^7) were transfected with expression vectors Flag-tIRF3 (5 μg) and HA–tSTING-FL (5 μg) or HA–tSTING-mini (5 μg) for 48 h, then infected with NDV (MOI = 1) at the indicated times. The procedures for immunoprecipitation (IP) and immunoblots (IB) were similar to Fig. 4D. (**D**) Colocalization of tSTING-mini and tIRF3 in response to NDV infection. TSPRCs (1×10^4) were transfected with vector tSTING-mini-EGFP (0.5 μg) for 48 h, followed by NDV infection (MOI = 1) at the indicated times. tIRF3 was immunostained by using anti-IRF3 Ab. All immunoblots and images are representative of three independent experiments with similar results. Scale bars, 10 μm.

infection (Fig. 4E). Overexpression of tagged tSTING-mini also interacted with the downstream adaptor tMAVS of the RLR (RIG-I–like receptors) signaling (Fig. 4F). Collectively, we found that the interaction of tSTING-mini and tMDA5–tLGP2 was sustained for a shorter time than that of tSTING-FL and tMDA5–tLGP2, but this association had a significantly stronger activation effect than that of tSTING-FL in response to RNA virus infection.

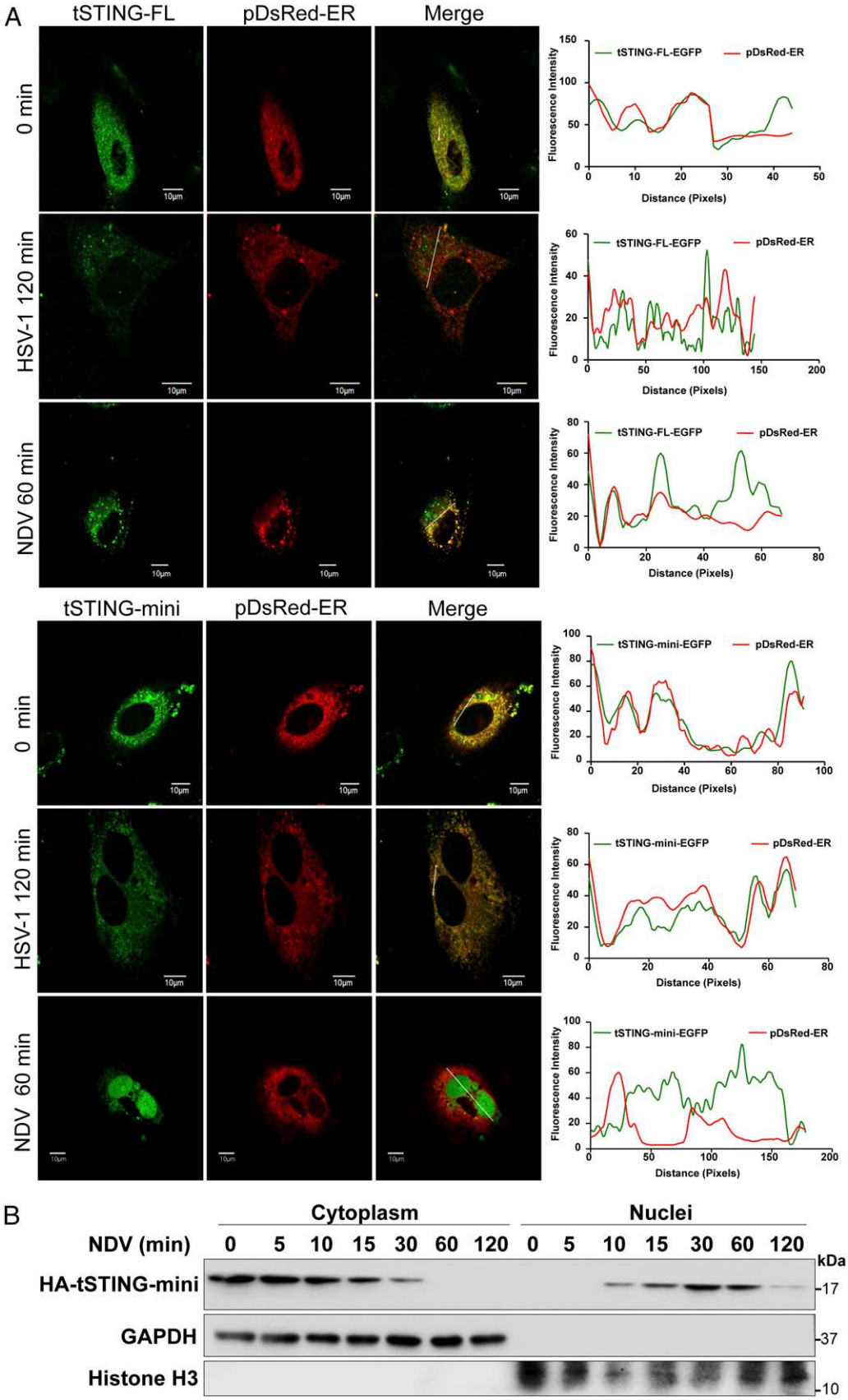

FIGURE 6. Alteration of subcellular localization of tSTING in response to viral infection. (**A**) Alteration of subcellular localization of tSTING during HSV-1 or NDV infection. TSPRCs (1×10^4) were cotransfected with tSTING-FL–EGFP (0.5 μg) or tSTING-mini-EGFP (0.5 μg) expression vector and pDsRed-ER vector (0.05 μg) for 36 h, followed by infection with HSV-1 (MOI = 10) for 2 h or NDV (MOI = 1) for 1 h. (Left) The yellow staining indicated a colocalization of tSTING with ER. (Right) Line graph indicated fluorescence intensity across the white line marked in the cell on the left. The densitometry of immunofluorescence in the cell was determined by the ImageJ. Scale bars, 10 μm. (**B**) *(Figure legend continues)*

tSTING-mini mediated tIRF3 phosphorylation through tSTING-mini-tIRF3 interaction after RNA virus infection

STING can trigger the phosphorylation of TBK1 and IRF3 by VSV and SeV infections (4, 5). We found that tSTING-mini overexpression in TSPRCs infected with NDV significantly enhanced the activation of IFN-β-Luc mediated by tIRF3 (Fig. 5A), but not tTBK1 (Supplemental Fig. 3A). tSTING-mini overexpression activated the tIRF3 phosphorylation at an early time point (at 10 min) and peaked at 1 h after NDV infection in TSPRCs. However, tIRF3 was phosphorylated in TSPRCs transfected with tSTING-FL or empty vector during NDV infection at a later stage (at 30 min), and had a gradual increase of phosphorylated level (Fig. 5B). We observed a similar pattern of time-dependent phosphorylation for p65 of the NF-κB signaling in TSPRCs transfected with empty vector, tSTING-FL or tSTING-mini, irrespective of NDV infection (Fig. 5B). Overexpression of tSTING-mini bound to tIRF3 in uninfected cells; this association was rapid, markedly increased at 5 min, and had disappeared by 4 h after NDV infection (Fig. 5C). In contrast, overexpression of tSTING-FL in TSPRCs only interacted with tIRF3 at the later stage (after 1 h) during NDV infection (Fig. 5C). tSTING-mini could not be immunoprecipitated by tTBK1 (Supplemental Fig. 3B) and tSTING-FL (Supplemental Fig. 3C) at resting cells or during NDV infection (Supplemental Fig. 3D), whereas tSTING-FL did have an interaction with tTBK1 (Supplemental Fig. 3B). These results suggested that tSTING-mini interacted strongly with tIRF3 and promoted tIRF3 phosphorylation at an early stage after NDV infection.

Translocation of tSTING-mini into the nucleus upon RNA virus infection

Immunostaining assays were used to show if tSTING-mini was colocalized with tIRF3 in TSPRCs upon NDV infection. We showed tSTING-mini–EGFP was colocalized with tIRF3 and translocated into the nucleus in a time-dependent manner after NDV infection (Fig. 5D). We found that both tSTING-FL–EGFP and tSTING-mini–EGFP were located in the ER in resting TSPRCs (Fig. 6A), consistent with previous studies (4, 46, 47). After HSV-1 infection for 2 h, tSTING-FL-EGFP was detached from the ER and relocalized to form puncta structures in the cytoplasm. In contrast, tSTING-mini–EGFP was retained in the ER and had no change to its location upon HSV-1 infection (Fig. 6A). Interestingly, NDV infection partially detached tSTING-FL–EGFP from the ER and led to diffusion and formation of cellular puncta. The tSTING-mini–EGFP was detached from the ER upon NDV infection and translocated to the nucleus (Fig. 6A). Biochemical assays for cytoplasmic and nuclear proteins confirmed the translocation of tSTING-mini into the nucleus after NDV infection in TSPRCs (Fig. 6B). A fast degradation of tSTING-mini could be observed over time in nuclear and cytoplasmic fractions in NDV-infected TSPRCs (Fig. 6B). These data indicated that tSTING-mini was translocated from the cytoplasm to the nucleus and degrades rapidly following RNA virus infection.

Ubiquitination and proteasomal degradation of tSTING-mini was promoted by tDTX3L and tPARP9

So as to identify potential factors that mediate the rapid degradation of tSTING-mini, we infected TSPRCs overexpressing tSTING-mini with NDV, followed by treatment with or without MG132 (a proteasomal inhibitor) and 3-methyladenine (3-MA; an inhibitor of autophagy), respectively. We observed a higher level of tSTING-mini in TSPRCs with MG132 treatment than that of the control (DMSO) or 3-MA–treated cells, indicating that tSTING-mini underwent degradation during NDV infection by proteolysis (Fig. 7A). In addition, MG132 treatment led to an increased level of tSTING-mini in a dose-dependent manner (Fig. 7B).

The proteasome serves to degrade proteins following their conjugation to ubiquitin (48). The PARP9-DTX3L complex acted as an E3 ubiquitin ligase targeting to both host and pathogen to enhance the IFN signaling (49). We determined subcellular localization of endogenous tPARP9 and tDTX3L in TSPRCs with or without NDV infection. The tPARP9 was mainly located in the nucleus, whereas tDTX3L was mainly distributed in cytoplasm in resting cells. Upon NDV infection, the tDTX3L was translocated into the nucleus in a time-dependent manner (Supplemental Fig. 3F, 3G). This cytoplasm-to-nucleus shuttling upon NDV infection was consistent with the subcellular localization of this complex that underwent dynamic shuttling between the nucleus and the cytoplasm upon IFN-γ treatment (50). We therefore investigated whether tPARP9–tDTX3L targeted tSTING-mini. Overexpression of tPARP9–tDTX3L in TSPRCs caused a decreased level of tSTING-mini, whereas overexpression of tPARP9 or DTX3L alone had no such effect. The overexpression was sensitive to blockade by MG132 (Fig. 7C). We used siRNA to knockdown endogenous tPARP9 and tDTX3L (Supplemental Fig. 3H, 3I) and could obtain a good knockdown efficiency (up to 50%) for tPARP9 (sitPARP9-3#) and tDTX3L (sitDTX3L-2#), respectively. Knockdown of tPARP9–tDTX3L complex caused a significantly increased level of tSTING-mini, whereas knockdown of tPARP9 or DTX3L alone had no such an effect (Fig. 7D). Moreover, the level of tSTING-mini ubiquitination was substantially increased in the presence of tPARP9–tDTX3L but not tPARP9 or DTX3L (Fig. 7E). To investigate the form of the polyubiquitin chains linked to tSTING-mini, we used wild-type HA-ubiquitin and its mutants K48 and K63, which have a lysine residue at the 48th and 63rd positions, respectively. The ubiquitination of tSTING-mini induced by tPARP9–tDTX3L was detected predominantly in cells overexpressing wild-type HA-ubiquitin or K48 (Fig. 7E). These results indicated that tPARP9–tDTX3L conjugates K48-linked polyubiquitin chains with tSTING-mini.

Discussion

The recognition of nucleic acids is a general strategy used by a host to detect invading pathogens. STING has been established as a central component in the innate immune response to cytosolic DNA and RNA derived from pathogens (8, 9), whereas its role in RNA virus infection remains controversial (10, 19). Most recently, Franz and coworkers (20) reported a novel mechanism for a STING-dependent translation inhibition that restricts RNA virus replication. In this study, we took advantage of the Chinese tree shrew, which has several unique genetic features in its immune system (27), including having two STING isoforms, as a model to characterize the role of STING following RNA virus infection. We found that tSTING-mini, a short alternative splicing variant of the

Western blot for HA–tSTING-mini expression in the cytoplasmic and nuclear fractions from TSPRCs, which were transfected with HA–tSTING-mini for 36 h, followed with NDV infection at the indicated times. All immunoblots and images are representative of three independent experiments with similar results.

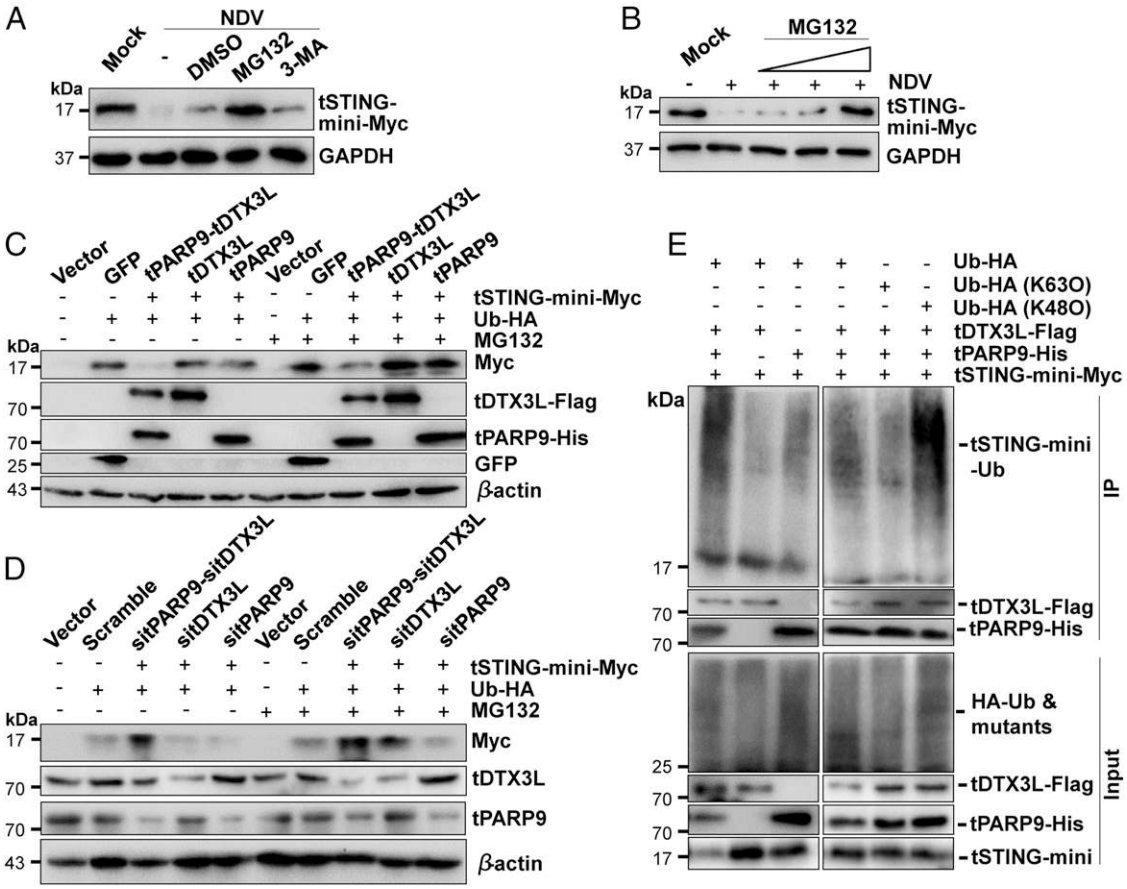

FIGURE 7. Ubiquitination and proteasome degradation of tSTING-mini is promoted by tPARP9–tDTX3L. (**A**) MG132, but not 3-MA, inhibited the NDV-induced tSTING-mini degradation in TSPRCs. Cells (1×10^6) were transfected with expression vector of tSTING-mini-Myc (2.5 μg) for 40 h and then treated with DMSO, MG132 (50 mM) or 3-MA (10 mM) for 4 h, respectively, followed by NDV infection (MOI = 1) or uninfected (Mock) for 3 h. Immunoblots for tSTING-mini and GAPDH were performed by using anti-Myc and anti-GAPDH Abs, respectively. (**B**) MG132 inhibited the NDV-induced degradation of tSTING-mini in a dose-dependent manner. The procedure was the same as (**A**), but with a dose-dependent treatment with MG132 treatment (2, 10, and 50 mM) and NDV infection for 3 h. (**C**) Immunoblot of tSTING-mini-Myc in TSPRCs with overexpression of tPARP9–tDTX3L, tPARP9, or tDTX3L. Cells (1×10^6) were cotransfected with expression vector of GFP (0.8 μg), tPARP9–tDTX3L (0.4 μg), tPARP9 (0.8 μg), or tDTX3L (0.8 μg), together with vectors tSTING-mini–Myc (0.8 μg) and HA-tagged ubiquitin (HA-Ub, 0.8 μg) for 40 h. Cells were then treated with or without MG132 (50 mM) for 8 h and infected with NDV 2 h before the harvest. (**D**) Immunoblot of tSTING-mini-Myc in TSPRCs with knockdown of tPARP9–tDTX3L, tPARP9, or tDTX3L. Cells (1×10^6) were cotransfected with sitPARP9–sitDTX3L (each 100 μM), sitPARP9 (100 μM), or sitDTX3L (100 μM), together with expression vectors tSTING-mini-Myc (0.8 μg) and HA-tagged ubiquitin (HA-Ub, 0.8 μg) for 36 h. Cells were then treated as in (**C**). (**E**) Overexpression of tPARP9–tDTX3L promoted tSTING-mini degradation via K48-linked polyubiquitination in TSPRCs. TSPRCs (1×10^7) were cotransfected with different combinations of expression vectors for tSTING-mini-Myc (6 μg), tPARP9–tDTX3L (each 1 μg), tPARP9 (2 μg), tDTX3L (2 μg), and HA-Ub or its mutants (2 μg) for 48 h. Cell lysates (Input) were immunoprecipitated (IP) by using anti-Myc Ab. Immunoblots (IB) for tSTING-mini, tPARP9, tDTX3L, and Ub were performed by using anti-Myc, anti-His, anti-Flag and anti-HA Abs, respectively. Data are representative of three independent experiments with similar results.

canonical tSTING, plays a critical role in restricting the RNA virus-induced signaling cascade. Overexpression of tSTING-mini activated the type I IFNs and IFN-stimulated genes and resulted in a very significant increase in tMDA5–tLGP2-mediated antiviral signaling after RNA virus infection, thereby providing a new mechanism for tSTING to restrict RNA virus replication by the phenomenon of alternative splicing.

STING has been shown to play an essential role in DNA virus and RNA virus induced signaling transduction in other vertebrate species, such as fish (51) and chicken (52). Similarly, we found that tSTING-FL is involved in the RNA virus-induced IFN induction pathway in the Chinese tree shrew, but its effect was inferior to that of tSTING-mini (Figs. 2, 3). There are three reasons as to why tSTING-mini initiates a faster and stronger anti-RNA virus response than tSTING-FL. First, tSTING-mini binds with tMDA5–tLGP2, tMDA5, and tMAVS in resting cells, whereas tSTING-FL does not bind to these proteins without viral infection (Fig. 4D–F). Second, tMDA5 activates the tSTING-mini–mediated signaling in a stronger and earlier way than the tSTING-FL–mediated signaling (Supplemental Fig. 3E). Moreover, tLGP2 has a stronger enhancing effect on tMDA5–tSTING-mini than on tMDA5–tSTING-FL–mediated antiviral signaling (Fig. 4A–C). Third, tSTING-mini, but not tSTING-FL, is able to promote tIRF3 phosphorylation upon RNA virus infection (Fig. 5B) without tTBK1 recruitment (Supplemental Fig. 3D). These results explain (at least partially) why tSTING-mini can modulate antiviral immunity in a faster and stronger way after a RNA virus infection. Further investigations should be carried out to explore the mechanism underlying tSTING-mini-mediated activation of IFN signaling without the involvement of TBK1.

Another interesting observation was the nuclear translocation of tSTING-mini after a RNA virus infection (Figs. 5D, 6). tSTING-mini interacted with tIRF3 in resting cells and the interaction was rapid and appeared within 5 min after NDV infection (Fig. 5C),

faster than the nuclear translocation of tSTING-mini (Fig. 6B). We speculate that nuclear translocation of tSTING-mini is caused by a hitchhiking effect of the cytoplasm-to-nucleus shuttling of tIRF3 after NDV infection, as the latter contained a nucleus localization signal (53). Note that we found a fast degradation of tSTING-mini after its translocation to the nucleus upon RNA virus infection, and this K48-mediated degradation to ubiquitin was promoted by tDTX3L–tPARP9 (Fig. 7), suggesting that tDTX3L–tPARP9 was a E3 ubiquitin ligase targeting tSTING-mini. This result was similar to a previous observation that PARP9–DTX3L could interact with STAT1 and enhanced translocation of STAT1 into the nucleus (49). However, it remained unclear whether the nuclear-cytoplasmic shuttling of tSTING-mini was essential for fast tIRF3 phosphorylation or whether the nuclear shuttling of tSTING-mini was associated with PARP9–DTX3L-mediated ubiquitination in a proteasome-dependent pathway. It should be mentioned that endogenous interaction between tSTING-mini with other cellular factors at the resting state and during RNA virus infection could not be performed due to the lack of specific Ab for tSTING-mini, although these results will enhance the biological relevance of the study.

Alternative splicing of an individual gene has the ability to generate multiple mRNAs that encode proteins with diverse and even antagonistic functions, and the shorter isoform fine-tuned signaling was a common mechanism observed during the RLR signaling (3), for example, short isoforms of human RIG-I [with a short deletion of the 36th–80th residues (54)], TBK1 [lacking exon 3–6 (55)], MAVS (56), and STING [STING-β, lacking exon 1–5 (57) and MRP, lacking exon 7 (58)]. Intriguingly, the tSTING-mini is shown to have a different regulatory role as compared with the human short STING isoform MRP (58) or STING-β (57). First, MRP harbored all four TMs and the dimerization domain but no TBK1-binding domain. Therefore, MRP could form homo- and heterodimers with itself and/or with STING but did not interact with TBK1 (58). tSTING-mini lacks both domains (Fig. 1A) and did not interact with tTBK1 (Supplemental Fig. 3B, 3D) or form heterodimer with tSTING-FL (Supplemental Fig. 3C). Second, overexpression of MRP inhibited STING-mediated activation of IFN-β by SeV infection or cyclic diguanylate treatment and enhanced the activation of IFN-β upon HSV-1 infection (58). The STING-β dominantly inhibited innate nucleic acid sensing (57). Conversely, overexpression of tSTING-mini enhanced NDV- and SeV-induced activation of IFN-β, potently reduced VSV-GFP replication, but had no significant effect on HSV-1 infection (Figs. 2, 3). Third, MRP expression was reduced after SeV infection but was upregulated after HSV-1 infection (58), whereas tSTING-mini has an opposite expression pattern in response to HSV-1 and RNA virus (NDV and SeV) infections (Fig. 2). Fourth, MRP retained the ability to interact with inducible inhibitor of NF-κB (IκB) and activated the NF-κB pathway (58), whereas tSTING-mini enhances the tMDA5- or tMDA5–tLGP2-mediated antiviral signaling after RNA virus infection (Fig. 4) and promotes tIRF3 phosphorylation through tSTING-mini–tIRF3 interaction (Fig. 5). All these data have suggested that there is a species-specific role of short STING isoform in the Chinese tree shrew and human in RNA virus-induced signaling, which also reflects diverse regulation of the innate immunity system.

In summary, we have found two STING isoforms in the Chinese tree shrew, which have markedly different functions in response to DNA virus and RNA virus infections. We have shown the molecular mechanism by which tSTING-mini positively regulates the anti-RNA virus response. Our study has offered a model concerning the role of STING in RNA virus infection via alternative splicing and illustrates a unique picture of the innate immunity system in the Chinese tree shrew.

Acknowledgments

We thank Dr. Ian Logan and Dr. Xin Wang (Ocean University of China) for helpful discussions and the staff at the Kunming Biological Diversity Regional Center of Instruments, KIZ for technical help with the flow cytometry assay.

Disclosures

The authors have no financial conflicts of interest.

References

1. Kawai, T., and S. Akira. 2006. Innate immune recognition of viral infection. *Nat. Immunol.* 7: 131–137.
2. Wu, J., and Z. J. Chen. 2014. Innate immune sensing and signaling of cytosolic nucleic acids. *Annu. Rev. Immunol.* 32: 461–488.
3. Carpenter, S., E. P. Ricci, B. C. Mercier, M. J. Moore, and K. A. Fitzgerald. 2014. Post-transcriptional regulation of gene expression in innate immunity. *Nat. Rev. Immunol.* 14: 361–376.
4. Ishikawa, H., and G. N. Barber. 2008. STING is an endoplasmic reticulum adaptor that facilitates innate immune signalling. [Published erratum appears in 2008 *Nature* 456: 274.] *Nature* 455: 674–678.
5. Zhong, B., Y. Yang, S. Li, Y.-Y. Wang, Y. Li, F. Diao, C. Lei, X. He, L. Zhang, P. Tien, and H.-B. Shu. 2008. The adaptor protein MITA links virus-sensing receptors to IRF3 transcription factor activation. *Immunity* 29: 538–550.
6. Jin, L., P. M. Waterman, K. R. Jonscher, C. M. Short, N. A. Reisdorph, and J. C. Cambier. 2008. MPYS, a novel membrane tetraspanner, is associated with major histocompatibility complex class II and mediates transduction of apoptotic signals. *Mol. Cell. Biol.* 28: 5014–5026.
7. Sun, W., Y. Li, L. Chen, H. Chen, F. You, X. Zhou, Y. Zhou, Z. Zhai, D. Chen, and Z. Jiang. 2009. ERIS, an endoplasmic reticulum IFN stimulator, activates innate immune signaling through dimerization. *Proc. Natl. Acad. Sci. USA* 106: 8653–8658.
8. Ran, Y., H. B. Shu, and Y. Y. Wang. 2014. MITA/STING: a central and multifaceted mediator in innate immune response. *Cytokine Growth Factor Rev.* 25: 631–639.
9. Liu, X., and C. Wang. 2016. The emerging roles of the STING adaptor protein in immunity and diseases. *Immunology* 147: 285–291.
10. Ishikawa, H., Z. Ma, and G. N. Barber. 2009. STING regulates intracellular DNA-mediated, type I interferon-dependent innate immunity. *Nature* 461: 788–792.
11. McWhirter, S. M., R. Barbalat, K. M. Monroe, M. F. Fontana, M. Hyodo, N. T. Joncker, K. J. Ishii, S. Akira, M. Colonna, Z. J. Chen, et al. 2009. A host type I interferon response is induced by cytosolic sensing of the bacterial second messenger cyclic-di-GMP. *J. Exp. Med.* 206: 1899–1911.
12. Burdette, D. L., K. M. Monroe, K. Sotelo-Troha, J. S. Iwig, B. Eckert, M. Hyodo, Y. Hayakawa, and R. E. Vance. 2011. STING is a direct innate immune sensor of cyclic di-GMP. *Nature* 478: 515–518.
13. Jin, L., K. K. Hill, H. Filak, J. Mogan, H. Knowles, B. Zhang, A. L. Perraud, J. C. Cambier, and L. L. Lenz. 2011. MPYS is required for IFN response factor 3 activation and type I IFN production in the response of cultured phagocytes to bacterial second messengers cyclic-di-AMP and cyclic-di-GMP. *J. Immunol.* 187: 2595–2601.
14. Abe, T., and G. N. Barber. 2014. Cytosolic-DNA-mediated, STING-dependent proinflammatory gene induction necessitates canonical NF-κB activation through TBK1. *J. Virol.* 88: 5328–5341.
15. Tanaka, Y., and Z. J. Chen. 2012. STING specifies IRF3 phosphorylation by TBK1 in the cytosolic DNA signaling pathway. *Sci. Signal.* 5: ra20.
16. Sauer, J. D., K. Sotelo-Troha, J. von Moltke, K. M. Monroe, C. S. Rae, S. W. Brubaker, M. Hyodo, Y. Hayakawa, J. J. Woodward, D. A. Portnoy, and R. E. Vance. 2011. The N-ethyl-N-nitrosourea-induced Goldenticket mouse mutant reveals an essential function of Sting in the in vivo interferon response to *Listeria monocytogenes* and cyclic dinucleotides. *Infect. Immun.* 79: 688–694.
17. Chen, H., H. Sun, F. You, W. Sun, X. Zhou, L. Chen, J. Yang, Y. Wang, H. Tang, Y. Guan, et al. 2011. Activation of STAT6 by STING is critical for antiviral innate immunity. *Cell* 147: 436–446.
18. Rasmussen, S. B., K. A. Horan, C. K. Holm, A. J. Stranks, T. C. Mettenleiter, A. K. Simon, S. B. Jensen, F. J. Rixon, B. He, and S. R. Paludan. 2011. Activation of autophagy by α-herpesviruses in myeloid cells is mediated by cytoplasmic viral DNA through a mechanism dependent on stimulator of IFN genes. *J. Immunol.* 187: 5268–5276.
19. Li, X.-D., J. Wu, D. Gao, H. Wang, L. Sun, and Z. J. Chen. 2013. Pivotal roles of cGAS-cGAMP signaling in antiviral defense and immune adjuvant effects. *Science* 341: 1390–1394.
20. Franz, K. M., W. J. Neidermyer, Y.-J. Tan, S. P. J. Whelan, and J. C. Kagan. 2018. STING-dependent translation inhibition restricts RNA virus replication. *Proc. Natl. Acad. Sci. USA* 115: E2058–E2067.
21. Aguirre, S., A. M. Maestre, S. Pagni, J. R. Patel, T. Savage, D. Gutman, K. Maringer, D. Bernal-Rubio, R. S. Shabman, V. Simon, et al. 2012. DENV inhibits type I IFN production in infected cells by cleaving human STING. *PLoS Pathog.* 8: e1002934.

22. Yu, C. Y., T. H. Chang, J. J. Liang, R. L. Chiang, Y. L. Lee, C. L. Liao, and Y. L. Lin. 2012. Dengue virus targets the adaptor protein MITA to subvert host innate immunity. *PLoS Pathog.* 8: e1002780.
23. Ding, Q., X. Cao, J. Lu, B. Huang, Y.-J. Liu, N. Kato, H.-B. Shu, and J. Zhong. 2013. Hepatitis C virus NS4B blocks the interaction of STING and TBK1 to evade host innate immunity. *J. Hepatol.* 59: 52–58.
24. Nitta, S., N. Sakamoto, M. Nakagawa, S. Kakinuma, K. Mishima, A. Kusano-Kitazume, K. Kiyohashi, M. Murakawa, Y. Nishimura-Sakurai, S. Azuma, et al. 2013. Hepatitis C virus NS4B protein targets STING and abrogates RIG-I-mediated type I interferon-dependent innate immunity. *Hepatology* 57: 46–58.
25. Holm, C. K., S. H. Rahbek, H. H. Gad, R. O. Bak, M. R. Jakobsen, Z. Jiang, A. L. Hansen, S. K. Jensen, C. Sun, M. K. Thomsen, et al. 2016. Influenza A virus targets a cGAS-independent STING pathway that controls enveloped RNA viruses. *Nat. Commun.* 7: 10680.
26. Aguirre, S., P. Luthra, M. T. Sanchez-Aparicio, A. M. Maestre, J. Patel, F. Lamothe, A. C. Fredericks, S. Tripathi, T. Zhu, J. Pintado-Silva, et al. 2017. Dengue virus NS2B protein targets cGAS for degradation and prevents mitochondrial DNA sensing during infection. *Nat. Microbiol.* 2: 17037.
27. Fan, Y., Z.-Y. Huang, C.-C. Cao, C.-S. Chen, Y.-X. Chen, D.-D. Fan, J. He, H.-L. Hou, L. Hu, X.-T. Hu, et al. 2013. Genome of the Chinese tree shrew. *Nat. Commun.* 4: 1426.
28. Yao, Y.-G. 2017. Creating animal models, why not use the Chinese tree shrew (*Tupaia belangeri chinensis*)? *Zool. Res.* 38: 118–126.
29. Amako, Y., K. Tsukiyama-Kohara, A. Katsume, Y. Hirata, S. Sekiguchi, Y. Tobita, Y. Hayashi, T. Hishima, N. Funata, H. Yonekawa, and M. Kohara. 2010. Pathogenesis of hepatitis C virus infection in *Tupaia belangeri*. *J. Virol.* 84: 303–311.
30. Li, L., Z. Li, E. Wang, R. Yang, Y. Xiao, H. Han, F. Lang, X. Li, Y. Xia, F. Gao, et al. 2015. Herpes simplex virus 1 infection of tree shrews differs from that of mice in the severity of acute infection and viral transcription in the peripheral nervous system. *J. Virol.* 90: 790–804.
31. Xu, L., D. Yu, Y. Fan, L. Peng, Y. Wu, and Y.-G. Yao. 2016. Loss of RIG-I leads to a functional replacement with MDA5 in the Chinese tree shrew. *Proc. Natl. Acad. Sci. USA* 113: 10950–10955.
32. Yu, D., Y. Wu, L. Xu, Y. Fan, L. Peng, M. Xu, and Y.-G. Yao. 2016. Identification and characterization of toll-like receptors (TLRs) in the Chinese tree shrew (*Tupaia belangeri chinensis*). *Dev. Comp. Immunol.* 60: 127–138.
33. Fan, Y., M. S. Ye, J. Y. Zhang, L. Xu, D. D. Yu, T. L. Gu, Y. L. Yao, J. Q. Chen, L. B. Lv, P. Zheng, et al. 2019. Chromosomal level assembly and population sequencing of the Chinese tree shrew genome. *Zool. Res.* 40: 506–521.
34. Guo, W. N., B. Zhu, L. Ai, D. L. Yang, and B. J. Wang. 2018. Animal models for the study of hepatitis B virus infection. *Zool. Res.* 39: 25–31.
35. Xu, X., H. Chen, X. Cao, and K. Ben. 2007. Efficient infection of tree shrew (*Tupaia belangeri*) with hepatitis C virus grown in cell culture or from patient plasma. *J. Gen. Virol.* 88: 2504–2512.
36. Wang, Q., P. Schwarzenberger, F. Yang, J. Zhang, J. Su, C. Yang, J. Cao, C. Ou, L. Liang, J. Shi, et al. 2012. Experimental chronic hepatitis B infection of neonatal tree shrews (*Tupaia belangeri chinensis*): a model to study molecular causes for susceptibility and disease progression to chronic hepatitis in humans. *Virol. J.* 9: 170.
37. Walter, E., R. Keist, B. Niederöst, I. Pult, and H. E. Blum. 1996. Hepatitis B virus infection of *tupaia* hepatocytes in vitro and in vivo. *Hepatology* 24: 1–5.
38. Yan, R. Q., J. J. Su, D. R. Huang, Y. C. Gan, C. Yang, and G. H. Huang. 1996. Human hepatitis B virus and hepatocellular carcinoma. I. Experimental infection of tree shrews with hepatitis B virus. *J. Cancer Res. Clin. Oncol.* 122: 283–288.
39. Xie, Z. C., J. I. Riezu-Boj, J. J. Lasarte, J. Guillen, J. H. Su, M. P. Civeira, and J. Prieto. 1998. Transmission of hepatitis C virus infection to tree shrews. *Virology* 244: 513–520.
40. Zhang, L., Z. L. Shen, Y. Feng, D. Q. Li, N. N. Zhang, Y. Q. Deng, X. P. Qi, X. M. Sun, J. J. Dai, C. G. Yang, et al. 2019. Infectivity of Zika virus on primary cells support tree shrew as animal model. *Emerg. Microbes Infect.* 8: 232–241.
41. Xu, S., X. Li, J. Yang, Z. Wang, Y. Jia, L. Han, L. Wang, and Q. Zhu. 2019. Comparative pathogenicity and transmissibility of pandemic H1N1, avian H5N1, and human H7N9 influenza viruses in tree shrews. *Front. Microbiol.* 10: 2955.
42. Yu, D., L. Xu, X. H. Liu, Y. Fan, L. B. Lü, and Y. G. Yao. 2014. Diverse interleukin-7 mRNA transcripts in Chinese tree shrew (*Tupaia belangeri chinensis*). *PLoS One* 9: e99859.
43. Xu, L., D. Yu, L. Peng, Y. Fan, J. Chen, Y.-T. Zheng, C. Wang, and Y.-G. Yao. 2015. Characterization of a MAVS ortholog from the Chinese tree shrew (*Tupaia belangeri chinensis*). *Dev. Comp. Immunol.* 52: 58–68.
44. Ran, F. A., P. D. Hsu, J. Wright, V. Agarwala, D. A. Scott, and F. Zhang. 2013. Genome engineering using the CRISPR-Cas9 system. *Nat. Protoc.* 8: 2281–2308.
45. Gu, T., D. Yu, Y. Li, L. Xu, Y. L. Yao, and Y. G. Yao. 2019. Establishment and characterization of an immortalized renal cell line of the Chinese tree shrew (*Tupaia belangeri chinesis*). *Appl. Microbiol. Biotechnol.* 103: 2171–2180.
46. Woodward, J. J., A. T. Iavarone, and D. A. Portnoy. 2010. c-di-AMP secreted by intracellular *Listeria monocytogenes* activates a host type I interferon response. *Science* 328: 1703–1705.
47. Saitoh, T., N. Fujita, T. Hayashi, K. Takahara, T. Satoh, H. Lee, K. Matsunaga, S. Kageyama, H. Omori, T. Noda, et al. 2009. Atg9a controls dsDNA-driven dynamic translocation of STING and the innate immune response. *Proc. Natl. Acad. Sci. USA* 106: 20842–20846.
48. Finley, D. 2009. Recognition and processing of ubiquitin-protein conjugates by the proteasome. *Annu. Rev. Biochem.* 78: 477–513.
49. Zhang, Y., D. Mao, W. T. Roswit, X. Jin, A. C. Patel, D. A. Patel, E. Agapov, Z. Wang, R. M. Tidwell, J. J. Atkinson, et al. 2015. PARP9-DTX3L ubiquitin ligase targets host histone H2BJ and viral 3C protease to enhance interferon signaling and control viral infection. *Nat. Immunol.* 16: 1215–1227.
50. Juszczynski, P., J. L. Kutok, C. Li, J. Mitra, R. C. Aguiar, and M. A. Shipp. 2006. BAL1 and BBAP are regulated by a gamma interferon-responsive bidirectional promoter and are overexpressed in diffuse large B-cell lymphomas with a prominent inflammatory infiltrate. *Mol. Cell. Biol.* 26: 5348–5359.
51. Xu, X., M. Li, Z. Wu, H. Wang, L. Wang, K. Huang, X. Liu, Q. Hou, G. Lin, and C. Hu. 2017. Endoplasmic reticulum transmembrane proteins ZDHHC1 and STING both act as direct adaptors for IRF3 activation in *Teleost*. *J. Immunol.* 199: 3623–3633.
52. Cheng, Y., Y. Sun, H. Wang, Y. Yan, C. Ding, and J. Sun. 2015. Chicken STING mediates activation of the IFN gene independently of the *RIG-I* gene. *J. Immunol.* 195: 3922–3936.
53. Kumar, K. P., K. M. McBride, B. K. Weaver, C. Dingwall, and N. C. Reich. 2000. Regulated nuclear-cytoplasmic localization of interferon regulatory factor 3, a subunit of double-stranded RNA-activated factor 1. *Mol. Cell. Biol.* 20: 4159–4168.
54. Gack, M. U., A. Kirchhofer, Y. C. Shin, K. S. Inn, C. Liang, S. Cui, S. Myong, T. Ha, K. P. Hopfner, and J. U. Jung. 2008. Roles of RIG-I N-terminal tandem CARD and splice variant in TRIM25-mediated antiviral signal transduction. *Proc. Natl. Acad. Sci. USA* 105: 16743–16748.
55. Deng, W., M. Shi, M. Han, J. Zhong, Z. Li, W. Li, Y. Hu, L. Yan, J. Wang, Y. He, et al. 2008. Negative regulation of virus-triggered IFN-beta signaling pathway by alternative splicing of TBK1. *J. Biol. Chem.* 283: 35590–35597.
56. Brubaker, S. W., A. E. Gauthier, E. W. Mills, N. T. Ingolia, and J. C. Kagan. 2014. A bicistronic MAVS transcript highlights a class of truncated variants in antiviral immunity. *Cell* 156: 800–811.
57. Wang, P.-H., S.-Y. Fung, W.-W. Gao, J.-J. Deng, Y. Cheng, V. Chaudhary, K.-S. Yuen, T.-H. Ho, C.-P. Chan, Y. Zhang, et al. 2018. A novel transcript isoform of STING that sequesters cGAMP and dominantly inhibits innate nucleic acid sensing. *Nucleic Acids Res.* 46: 4054–4071.
58. Chen, H., R. Pei, W. Zhu, R. Zeng, Y. Wang, Y. Wang, M. Lu, and X. Chen. 2014. An alternative splicing isoform of MITA antagonizes MITA-mediated induction of type I IFNs. *J. Immunol.* 192: 1162–1170.